Testing 3D landform quantification methods with synthetic drumlins in a real digital elevation model

J. K. Hillier[a*] and M. J. Smith[b] [*]Corresponding Author
[a]Department of Geography, Loughborough University, LE11 3TU, UK. j.hillier@lboro.ac.uk.
tel: 0044 (0)1509 223727 fax: 0044 (0)1509 223930
[b]School of Geography, Earth and the Environment, Kingston University, KT1 2EE, UK.
mike@hsm.org.uk

Metrics such as height and volume quantifying the 3D morphology of landforms are important observations that reflect and constrain Earth surface processes. Errors in such measurements are, however, poorly understood. A novel approach, using statistically valid 'synthetic' landscapes to quantify the errors is presented. The utility of the approach is illustrated using a case study of 184 drumlins observed in Scotland as quantified from a Digital Elevation Model (DEM) by the 'cookie cutter' extraction method. To create the synthetic DEMs, observed drumlins were removed from the measured DEM and replaced by elongate 3D Gaussian ones of equivalent dimensions positioned randomly with respect to the 'noise' (e.g. trees) and regional trends (e.g. hills) that cause the errors. Then, errors in the cookie cutter extraction method were investigated by using it to quantify these 'synthetic' drumlins, whose location and size is known. Thus, the approach determines which key metrics are recovered accurately. For example, mean height of 6.8 m is recovered poorly at 12.5 ± 0.6 (2σ) m, but mean volume is recovered correctly. Additionally, quantification methods can be compared: A variant on the cookie cutter using an un-tensioned spline induced about twice (×1.79) as much error. Finally, a previously reportedly statistically significant (p = 0.007) difference in mean volume between sub-populations of different ages, which may reflect formational processes, is demonstrated to be only 30–50 % likely to exist in reality. Critically, the synthetic DEMs are demonstrated to realistically model parameter recovery, primarily because they are still almost entirely the original landscape.

Results are insensitive to the exact method used to create the synthetic DEMs, and the approach could be readily adapted to assess a variety of landforms (e.g. craters, dunes, volcanoes).

Key words: synthetic, landform, DEM, drumlin, volume

1. Introduction

The 3D properties of landforms record information about the processes that formed them (e.g. Evans, 1987; Rose, 1989; Marova, 2002). Specifically, drumlins' heights, *H,* and volumes, *V,* may preserve information about the dynamics of former ice sheets (e.g. Smith et al., 2009). Quantification of these metrics (e.g. Smith et al., 2009), however, is prone to inaccuracy in the presence of topographic 'noise' (e.g. trees, post-formational erosion) and underlying larger-scale slopes (e.g. hills). So, observations like recovered mean height ($\overline{H}_r$) might be substantially overestimated and reflect noise rather than ice sheet processes. Without precise, accurate and reliable observations scientific conclusions based upon them must remain in some doubt. A fundamental question then arises of how to test quantification methods. What is the correct answer to test against? Like many classes of landform, the geometric rules used to map drumlins (e.g. Shaw, 1983; Rose, 1987; Smith and Clark, 2005; Clark et al., 2009; Spagnolo et al., 2010) are not yet definitively defined. So, establishing an objective *a priori* correct ground-truth with which to test the quantitative methods is not possible. It is not possible to conduct a careful manual interpretation, or an analysis using visually assessed numerical methods, and claim this as to be the 'correct' *H* or *V*. Either would just be one estimate, based on a number of implicit or explicit assumptions. Subsequent tests to determine which computational method best reproduced these 'correct' values would then simply indicate the method that best reproduced the underlying subjective preferences. This can, and has (e.g. Hillier, 2008), been done but is not a truly objective assessment. In these circumstances it is standard best-practice to test the method with some idealised or 'synthetic' data such as the classic 'synthetic checkerboard' test (e.g. Dziewonski et al., 1977, Saygin and Kennett, 2010) used extensively in Earth tomography. The constituent stages of this test (Nolet et al., 2007) illustrate the key elements of a synthetic test

1. *Construct a synthetic input*, which should include the feature of interest. In geomorphology, this could be the expected morphology of a landform.
2. *Create synthetic data* that resembles the observed data, with suitable noise added. In geomorphology, this could be a DEM including the synthetic input.
3. *Invert synthetic data* using the same numerical method applied to the observed data
4. *Compare inverted result with the synthetic input* to see how well the assumed synthetic input (e.g. landform) is recovered.

In geomorphology, synthetic data have been used to assess numerical methods for estimating the fractal dimension of topography (Malinverno, 1989; Tate, 1998a,b), and slope and aspect (Zhou, 2004). The performance of filters intended to isolate submarine volcanoes has also been assessed by simplistically approximating them as cones on planar surfaces (Wessel, 1998; Hillier, 2008; Kim and Wessel, 2008). Realistic 'noise' and regional trends, however, have not been used to assess landform retrieval. Neither have methods to extract the 3D properties (e.g. height and volume) of other landforms yet been subject to testing with synthetic DEMs. The difficulty lies in generating a suitable, statistically representative synthetic landscape.

Synthetic DEMs may be constructed by i) using simple geometries as building blocks such as cones or planes (e.g. Wessel, 1997; Kim and Wessel, 1998; Zhou, 2004; Hillier, 2008) ii) generated statistically using fractals (e.g. Mandelbrot, 1983) or multi-fractals (e.g. Gilbert, 1989; Weissel, 1994; Cheng, 1996) or iii) created by the application of mathematical descriptions of physical processes in 'landscape evolution models' (e.g. Chase, 1992; Braun and Sambridge, 1997). Synthetic DEMs created using simple building blocks, do not contain the complexity in the observed landscape, or necessarily have realistic statistical properties. Even multi-fractal landscapes, may not have correct statistics without considering properties such as anisotropy (e.g. Gagon, 2006) and characteristic scales (e.g. Perron, 2008), but more importantly these DEMs will not contain spatially distinct, isolated features (e.g. drumlins). Landscape evolution models, which link form with process by applying mathematically characterisations of the processes, can now incorporate many processes (Tucker, 2010); for instance, stochastic bedrock landsliding (e.g. Densmore, 1998), flexural isostasy (e.g. Lane et al., 2008), and valley-scale erosion by ice flow (e.g. Harbour, 1992; Brocklehurst and Wipple, 2004; Amundson and Iverson, 2006; Tomkin, 2009), including under thermo-mechanically coupled 3D ice sheets (e.g. Jamieson et al., 2008). Numerical models, however, cannot as yet realistically generate some landforms such as drumlins (e.g. Hindmarsh, 1998; Schof, 2007; Fowler, 2000, 2009, 2010a, 2010b). The problem of creating a statistically representative synthetic landscape containing drumlins therefore remains a current one.

By whichever method synthetic DEMs are generated, if they are to be used in the assessment of morphological mapping or to test numerical methods for quantifying the 3D properties of landforms, a number of criteria must be satisfied. Firstly, the synthetic DEM must be quantitatively representative of the observed landscape, at least in the aspects of it being examined. This is necessary to comment upon process-related statements such as ‘landform sub-population A differs from sub-population B’. Synthetics partially reflecting the observed landscape will permit only a subset of inferences to be drawn. Of particular note is the difficulty of ‘noise’ (e.g. alignments of trees). Noise may not be well represented by statistical noise (e.g. Lombardini, 2005; Jordan and Watts, 2005; Sun, 2009) and its removal by ‘decluttering’ (e.g. Sithole and Vosselman, 2004) likely distorts the landforms. The second criterion is that circularity, the retrieval of input assumptions, must be avoided. For instance, synthetic DEMs should not contain signatures of any isolation method such as the cookie cutter that would cause it to be favoured when comparing isolation methods.

This paper proposes a method of testing 3D landform quantification techniques such as the cookie cutter. It is applicable to varied study areas without substantial customization, and is potentially applicable to various landforms (e.g. drumlins, dunes, scoria cones, landslides). It avoids *a priori* assumptions about process and permits analyses of synthetics that are directly and securely relevant to real study sites. These assertions are demonstrated using a worked example. The study area, DEM data and quantification method used are outlined in Section 2. The processes of creating and using the synthetic DEMs (Fig. 1) has four stages, listed below, corresponding to those enumerated above. These stages are explained sequentially in the paper.

1. To first-order isolate, remove, and parameterise landforms (i.e. drumlins) from the measured DEM (Sections 3.1 and 3.2). Then, establish their idealised 3D shape (Section 3.3).
2. Re-insert idealised landforms (i.e. drumlins) using parameters matching those removed into the 'synthetic' DEMs at locations that are random with respect to surface clutter and larger features (Section 3.4).
3. Run the quantification methodology under examination, i.e. the cookie cutter (Section 4)
4. See how it recovers *a priori* known parameters from the synthetic DEM (Section 5)

Some ways in which observations and scientific claims may be evaluated using synthetic DEMs are then illustrated through the worked example, assessing the 'cookie cutter' method of Smith et al. (2009) as applied to the drumlin field they analysed in central Scotland. The same DEM and manual digitisations of the drumlins' outlines are used so that a direct comparison is possible. To highlight the extent of the observational problem note that it is not known if important parameters, e.g. recovered mean volume ($\overline{V}_r$), reflect the actual population at all.

2. Study area, data, and extraction method to be tested

The study area is in the western part of central Scotland (Fig. 2a). It (Fig. 2c) is 13 × 8 km in size, is identical to that analysed by Smith et al. (2009), and completely contains 175 landforms interpreted by them as drumlins. These landforms are Younger Dryas (YD) [~12 ka] and Last Glacial Maximum (LGM) [~20 ka] in age (Rose and Smith, 2008). Smith et al. (2009) report that, using a t-test without assuming equal variances, the observed difference in mean volumes between YD and LGM drumlins is statistically significant. Specifically, this refers to a difference in the logarithms of volumes, $\Delta\overline{\ln(V)}$, calculated as $\overline{\ln(V)}_{LGM} - \overline{\ln(V)}_{YD}$.

As in Smith et al. (2009) the NEXTmap Britain™ digital surface model (DSM), or 'NEXTmap', is used in this study (Fig. 2b). NEXTmap is a single-pass interferometric synthetic aperture radar (IfSAR) product presented as a spatial (*x, y*) grid at a resolution of five metres, with a vertical resolution estimated as 0.5–1 m (Intermap, 2004). The 184 digitised drumlin outlines used are also those of Smith et al. (2009) (Fig. 2c). These were digitised from NEXTmap and quantitatively compared to field mapping in Smith et al. (2006). A combination of gradient, two orthogonal relief-shaded images, and local contrast visualizations, considered 'optimal' (Smith and Clark, 2005), was used in the digitisation to minimise bias in the orientations of the drumlins (Smith and Wise, 2007). Re-analysis of the digitised outlines of the 184 drumlins indicates that 178 drumlins (n = 178) have all vertices within the study area, and these are used as the basis for computation in this paper based on this criterion alone.

The semi-automated 'cookie cutter' method (Smith et al., 2009) estimates a basal surface by interpolating between points on manually digitised drumlins' outlines using a fully tensioned (i.e. T =1) bi-cubic spline (e.g. Smith and Wessel, 1990), thereby permitting drumlins' volumes (V) and maximum heights (H) to be estimated. Specifically, this is implemented here by considering each drumlin in turn, starting from complete data across a sub-region of the observed DEM and i) removing measured heights within the outline, then ii) interpolating across the 'hole' using the spline to estimate a basal surface, and finally iii) calculating *H* and *V*. *H* is the maximum vertical difference between the original and interpolated surfaces, and *V* as the volume between the surfaces. All calculations are at the full resolution of the DEM.

The cookie cutter is a 'regional-residual separation' (RRS) technique (e.g. Wessel, 1998; Hillier and Smith, 2008, Hillier, 2008). Distinctively for an RRS technique the cookie cutter alone requires a manually digitized outline as an input. This, however, permits a simple method and creates results fully compatible with the subjective digitisations that are predominant in sub-aerial geomorphology. The cookie cutter likely introduces highly significant, but un-quantified, errors in estimates of *H* and *V*, but as a numerical method it is reproducible with the potential for it to be quantitatively tested.

3. Method for creating the synthetic DEMs

This section describes the methods used during the steps to create the synthetic DEMs, which are outlined in Section 1.

3.1 Drumlin isolation and removal

Height, *H*, recorded in Digital Elevation Models (DEMs) can be described at any location (x, y) as the sum of n 'components' (Eq. 1) (e.g. Wren, 1973; Wessel, 1998; Hillier and Watts, 2004; Hillier and Smith, 2008).

Eq. (1) $H_{\mathrm{DEM}} = H_1 + H_2 + \ldots\ldots H_n$

Eq. (2) $H_{\mathrm{DEM}} = H_{\mathrm{noise}} + H_{\mathrm{drumlins}} + H_{\mathrm{hills}}$

The topography of the study area can be described by Eq. 2, where 'noise' consists of surface 'clutter'; small-scale height variations not genetically related to drumlin formation. Specifically, clutter includes features such as trees and houses resting upon the terrain, and post-glacial alterations. 'hills' is a shorthand for larger-scale trends and landforms that are not drumlins. Regional-residual separation into these components is conducted using two standard (e.g. Wessel, 1998) sliding-window median filters. This filter is chosen for its robustness to outliers, simplicity, so that no element of the cookie cutter method was involved in the creation of the synthetic DEMs. This was done to avoid any possibility of circularity.

Numerous inspections, such as that illustrated in Figs. 3 and 4a,b, were used to establish the best filter widths (60 m, 500 m) for this initial estimate of drumlins' 3D form. Note, however that it is not possible to objectively demonstrate that any RRS is optimal at this stage because no 'correct' interpretation is known to test against. The efficacy of the division into the three components is illustrated as follows: Drumlins are not visible in Fig. 3c, clutter is minimized in Fig. 3b, and drumlins are not visible in H_{hills} (Fig. 3d). Even for this best visual assessment, some undesirable behaviours still exist. For example, the basal surface estimated is higher than might be expected in places (Fig. 4a,b). The synthetic DEMs created using the filters selected, however, are shown to be sufficiently realistic in Section 6; *H* and *V* are extracted in the same way for the real and synthetic DEMs.

H_{drumlins} was subtracted from H_{DEM} within the digitised outlines to remove drumlins, but they will be replaced by similar objects within the landscape (Fig. 1, Section 3.4). Outside the digitized outlines the DEM was not altered, retaining all its spatial and statistical characteristics. Thus, the synthetic landscapes will closely resemble the original.

3.2. Drumlin parameterisation

Length (*L*), width (*W*), height (*H*), and volume (*V*) are the main parameters used to quantify drumlins. *L*-*W*-*H* triplets are needed to create idealised drumlins for the synthetic DEMs. *L* and *W* are properties of drumlins' planform shapes, but can be calculated several different ways.

Since drumlins' idealised planar shape remains debated (e.g. Corley, 1959; Shaw, 1983; Spagnolo et al., 2010), methods assuming an idealised shape are not used here. Instead, L and W are calculated directly from drumlins' manually digitised outlines. Errors and systematic baises due to any method chosen for this, and then to calculate H and V, are unavoidable. So, two contrasting methods were implemented (Appendix A) so that the sensitivity of parameters (θ_L, V, H, L, and W) to them can be assessed. These are referred to as 'Method 1' and 'Method 2'.

3.3. Representative 3D drumlin shape

Using an idealised shape for drumlins breaks the link between filters used to generate input H and V and the testing of recovery efficacy. Without this break some signature of these filters may remain, perhaps introducing circularity. What shape, however, is appropriate?

Drumlins can be described as 'an elongated hill or mound … possessing a smooth "moulded" outline' (Hollingsworth, 1931), and various analogies have been used to describe their geometry: e.g. half torpedo, tear drop, half egg, cigar (see Spagnolo, 2010). Shaw (1983) distinguishes three isolate forms, i.e. those not in contact with other forms: 'spindle', 'parabolic', and 'transverse asymmetrical'. Reed et al. (1962), however, remain alone in proposing a 3D form with a simple mathematical description, the ellipsoid. In ellipsoids, slopes increase towards their edges. This model does not fit in the Central Scotland study area where slopes appear to decrease (Fig. 4a,b).

To determine a representative 3D drumlin shape to use in creating synthetic landscapes transverse and longitudinal profiles from the drumlins were stretched to a standard size and overlain on each other i.e., de-cluttered, de-trended, normalised (Fig. 4c,d), and stacked (Fig. 5). To de-trend, the estimated basal surface was subtracted. To normalize, distances were linearly scaled such that L, W, and H all become 1.0. To stack, the mean and standard deviation of normalized heights at each normalized distance along the profile were computed. Note that all profiles start from θ_L (Fig. 6a) used so the longitudinal profiles all align, with C_{xy} to the right.

Visually, a Gaussian form (grey line) well approximates the average transverse profiles (Fig. 5b,d), i.e. is within $\pm 2\sigma_{\overline{H}}$, and is close to the longitudinal profile of Method 1. In accord with observations elsewhere (Spagnolo et al., 2010) the asymmetries for Method 2 are not strongly aligned with flow (Fig. 2c), and so Fig. 5c resembles Fig. 5a if drumlins are aligned to the interpreted regional flow direction before stacking. About 10% of the height change associated with the approximating Gaussians' amplitude is outside the grey box representing the drumlins' limits (Fig. 5). So, the upper 90% of an elongate Gaussian form (Fig. 7), $H_f = 0.9$, is taken as the representative 3D form for drumlins in this study area. Are the stacked profiles exactly Gaussian? Points along the observed curves (black lines) lack independence, rendering statistical tests (e.g. Chi-squared goodness of fit) of this invalid, but the question is also not particularly relevant. As above, the approximation is demonstrably sufficient because H and V are extracted in the same way for the real and synthetic DEMs. Reassuringly, volumes of idealised Gaussians (Eq. A.1, Fig. 7) and volumes from grid-based calculations, for Method 2 where direct comparison is possible, agree well visually (Fig. 8b) and correlate with an r^2 = 0.8724 (n = 173). So, the Gaussian approximation has no systematic effect upon input volumes, V_{in}.

3.4. Building synthetic DEMs

Using an idealised Gaussian shape (Appendix B), and parameters characterising the drumlins (Fig. 8), synthetic DEMs were created by removing existing drumlins and inserting idealised ones (Fig. 1). To avoid the non-trivial problem of statistically generating realistic H-W-L triplets the measured ones where $H > 0$ were used; n = 178 for Method 1 and n = 173 Method 2.

Complications avoided include i) the relative abundances of different sizes of *L*, *W*, *H* (Fig. 8c,d,e) and ii) the strength of correlations between *L*-*W*, *L*-*H* and *H*-*W* varying as a function of size. The spatial distribution of drumlins (Fig. 9a,b) was reproduced (Fig. 9 c,d), and the distribution of θ_L was replicated (Fig. 8a). Details of the exact procedures used are in Appendix C. For both Method 1 and Method 2 10 synthetic DEMs and sets of digital drumlin outlines, were created. It would also be possible to spatially vary the dominant orientation, making the synthetic more realistic. However, when analysed, *H* and *V* are extracted in the same way for the real and synthetic DEMs (Section 6). So neither this additional complexity, nor the inclusion of asymmetry in an idealised Gaussian shape, is necessary.

4. Method for using the synthetic DEMs to assess the cookie cutter

This section describes the methods used to interrogate the synthetic DEMs. To assess its ability to recover *H* and *V*, the cookie cutter was applied to each of the 20 synthetic landscapes. The heights and volumes of the idealised drumlins put into the synthetic DEMs are denoted H_{in} and V_{in}. Recovered heights are denoted, H_r, and volumes, V_r. In addition, analyses were repeated employing a variant of the cookie cutter method, using an un-tensioned (i.e. T = 0) rather than a tensioned (i.e. T = 1) spline. This test is designed to illustrate the utility of synthetic DEMs in assessing different extraction methodologies. The results of both tests are reported in Sections 5.1 to 5.3. Note that, for consistency, the same parameterisation method (e.g. Method 1) was used to quantify drumlins extracted by the cookie cutter as was used to create the synthetic DEM analysed.

Next, the types of investigation made possible by knowing both V_{in} and V_r for synthetic DEMs are illustrated. Their results are reported in Section 5.4. The first illustrative investigation assesses the likelihood that the difference in volume between YD and LGM drumlins reported by Smith et al. (2009) actually exists when errors that occur during the extraction of drumlins' volumes are considered. Standard statistical tests (e.g. Smith et al. 2009) implicitly assume that automated methods recover drumlins' parameters exactly. A sub-set of 100,000 stochastically generated pairs of LGM and YD sub-populations with 'observed' differences (i.e. $\Delta\overline{\ln(V_r)}$) extracted by the cookie cutter more extreme than that reported by Smith et al. (2009) was assessed to see what proportion of them had 'real' input differences (i.e. $\Delta\overline{\ln(V_{in})}$) over the threshold for 95% significance (i.e. $\Delta\overline{\ln(V)}_{crit}$). To paraphrase; If the difference you extract is at least as large as that reported by Smith et al. (2009), what fraction of the time is the actual difference large enough to be statistically significant? This is illustrated in Fig. 10, with details of the stochastic modelling in Appendix D.

A second investigation was also performed. It is possible that the observed $\Delta\overline{V}$ between sub-populations is due to how the cookie cutter method interacts with spatial variation in regional trends and topographic noise between the LGM and YD regions. This was tested. If the recovered difference in mean volumes between regions is consistently larger or smaller than that input, this is caused by a difference between them. The effect, E, that the process of landform extraction makes to the difference in mean volume between the LGM and YD areas (i.e. $\overline{V}_{LGM} - \overline{V}_{YD}$), was quantified as the change in difference between average volumes of the sub-populations between input and recovery, specifically

Eq. (3) $$E_V = \frac{1}{n}\sum_{i=1}^{n}(\Delta\overline{V}_r - \Delta\overline{V}_{in})_i$$

where i is the number of the DEM out of 10. $\Delta\overline{V}_r$ and $\Delta\overline{V}_{in}$ are retrieved and input volume differences respectively. Equivalent comparisons were made for $\Delta\overline{H}$, un-tensioned splines, and Methods 1 and 2.

5. Results

5.1 Negative volumes

For the 10 synthetic DEMs analysed using the cookie cutter and parameterised with Method 1, 14.3 ± 6.4 (2σ) of 178 drumlins have negative (i.e. incorrect) volumes. For Method 2 the equivalent number is similar, 15.4 ± 2.8 (2σ) of 173. Within error these are not distinguishable from the 11 negative volumes recovered by analysing the original DEM and its manually digitised outlines. This is a first indicator that the synthetic DEMs well replicate the original, at least when measuring H and V. Using an un-tensioned spline figures are 32.3 ± 7.6 (2σ) and 26.4 ± 9.2 (2σ) for Methods 1 and 2 respectively. So, these definite errors are significantly more numerous for the un-tensioned spline (e.g. $p = \sim 7\times10^{-10}$, Method 1, 1-tailed t-test assuming equal variances). This is initial evidence that the un-tensioned variant recovers H and V more poorly. Note that in hilly, noisy terrain large errors producing negative volumes are expected of interpolation using splines (e.g. Fig 11b of Smith et al. (2009)). Indeed, this is one of the main drivers behind this work to develop synthetic DEMs.

5.2 Individual heights and volumes

For Method 1 parameters, 39.2% of individual recovered volumes are within ×0.75 – 1.25 of V_{in}, i.e. V_r/V_{in} is in the range 0.75 to 1.25. Table 1 summarizes such results. Percentages are consistently higher for V than H, and for tensioned rather than un-tensioned variants for the cookie cutter. Consistent with this, standard deviations of V_r/V_{in} are notably smaller for tensioned as compared to un-tensioned splines, although this difference is much less marked for H_r/H_{in}. In short, on an individual basis drumlins' parameters are poorly recovered, especially for the un-tensioned spline. V_r values are distributed approximately symmetrically about their true values i.e. V_{in}, whilst recovered heights tend to be too great (Fig. 11). This determines how well population parameters are recovered (Section 5.3). The range 1±0.25 is arbitrarily chosen, but observations are consistent for other ranges e.g. 1±0.5. Figure 11 plots the shape of the distributions of V_r/V_{in} and H_r/H_{in}, and illustrates that large drumlins (black) are recovered in a similar way to the whole population. This is a necessary check that small, numerous drumlins are not dominating the results.

5.3 Population parameters

For the 10 groups of 178 drumlins, of parameters estimated by Method 1, mean input volume ($\overline{V}_{in}$) is 1.59 $\times 10^5$ m^3. Mean volume ($\overline{V}_r$) is recovered well as 1.56 ± 0.16 $\times 10^5$ m^3 (2 σ). The 10 $\overline{V}_r$ estimates are plotted in Figure 12b, and $\overline{V}_{in}$ is within the spread of these figures. Mean height ($\overline{H}_{in}$) of 6.8 m is poorly recovered as 12.5 ± 0.6 (2σ) m. $\overline{H}_{in}$ is not within the spread of $\overline{H}_r$. This is due to the strongly skewed distribution of errors for individual drumlins (Fig. 11 a,c). Results are similar for Method 2, and for both tensioned and un-tensioned splines (Table 2), and so the observations are robust.

5.4 Sub-populations

What is the effect of inaccuracies due to the cookie cutter method upon the conclusions of Smith et al. (2009)? This is the first investigation of sub-populations. For synthetics using Method 1, 715 of 100,000 simulations have observed volume differences $\Delta\overline{\ln(V_r)}$ more extreme than those observed by Smith et al. (2009). Of these only 42% of these have 'actual' input volume differences that are significant (i.e $\Delta\overline{\ln(V_{in})} > \Delta\overline{\ln(V)}_{crit}$). A duplicate analysis, but using Method 2, gives a value of 38%. A comparison with parametric statistics demonstrates the confidence that it is possible to have in the stochastic modelling. When inaccuracies in extracting the volumes are not considered they agree well. Specifically p values under H_0: $\overline{\ln(V_{LGM})} = \overline{\ln(V_{YD})}$ for a t-test that does not assume equal variances and the stochastic modelling are 0.0062 and 0.0071 respectively.

What is the effect upon population parameters of possible differences in the character of noise or hills between the two regions? This is the second investigation. Mean E_V values for Methods 1 and 2 (Table 3) quantify the systematic difference between areas. These are smaller than the 32,199 m^3 observed by Smith et al. (2009) or in the opposite direction. So, they cannot explain the observation of Smith et al. (2009), reassuringly suggesting that it is possible to see geomorphic signal through the noise. This main result is insensitive to method used or tension on the spline employed (Table 3). For height, in contrast, a systematic effect of ~1 m appeared consistently increasing heights for LGM drumlins more. This would have to considered were any claims made about differences in mean heights: For the data of Smith et al. (2009) the mean height of LGM drumlins is 3.0 m greater than YD, with a critical difference of only 2.0 m at the 95% confidence level calculated stochastically assuming accurate extraction.

6. Discussion

For a synthetic DEM to be useful, it must be statistically representative of the real DEM, at least for the scenario to be assessed. In this case, the scenario is the quantification of H and V using semi-automated methods. In the search for a best way of quantifying drumlins, by definition no *a priori* information is or can be available for parameters of the original, non-Gaussian drumlins in the DEM. So, the best test possible is to compare the shapes of recovered parameter populations (Fig. 13). For these to match closely either all stages of generating and processing the synthetic DEMs are correct or any significant errors that exist within these stages must have produced equal and opposite effects.

A number of attempts are made to falsify the idea that the synthetic DEMs well approximate the real landscape by comparing output from the cookie cutter method as applied to the original and synthetic DEMs. Firstly, the shapes of the populations of recovered volumes are examined quantitatively by inter-quartile ranges and skews, and visually (Fig. 13a). They are very similar. Thus, the idea that the synthetic DEMs well represent reality is not contradicted. Secondly, the shape of an input V distribution is modified, spread out, by errors in recovery (e.g. Fig. 13c). Similar numbers of negative volumes (Section 5.1), definite mistakes, for the real and synthetic datasets are therefore a strong direct indicator that DEMs are behaving similarly. Differences in the input distributions generated by Methods 1 and 2 (Fig. 8b), however, make this comparison inexact. The differences can, however, be corrected for by aligning mean recovered volumes ($\overline{V}_r$) (Fig. 13a). This is valid if errors in recovery are randomly distributed about their true values, as they appear to be (Fig. 11b,d). Thus if errors are random, if input distributions (e.g. Fig. 8b) are of the correct shape, and if parameters are recovered in the same way for the real and synthetic data, scaled curves for recovered volumes should overlie each other. They do (Fig. 13a). 'Scaling factors', are 0.82 and 1.17 for Methods 1 and 2 respectively. Thus, the idea that the synthetic DEMs well represent reality is again not contradicted. It is not obvious, however, that a combination of a different 'scaling factor' and errors of a different magnitude may be able to equally well approximate the shape of the distribution. So, thirdly, to discount the possibility that the fit occurred by chance due to a trade-off between effects, an inversion (Fig. 13b) was conducted. This examined all possible magnitudes of scaling factor and error magnitude as multiples of that actually found for the synthetic data: 'error multiplier'. Best-fit scaling factors of 0.82 and 1.14 were found for Methods 1 and 2, very similar to those used to align the means. Thus the fit between the curves does not appear arbitrary. The error multipliers, applied to V_{in}-V_{r} for individual drumlins that minimise misfit are 0.80 and 0.99 for Methods 1 and 2 respectively. These are again consistent with the idea that the synthetic DEMs well approximate reality, providing little evidence that results cannot be interpreted with confidence. An error multiplier of 0.80 suggests that analyses based on Method 1 may have errors that are ~20% too large, but this is affects results insufficient to alter any conclusions.

As for V, recovered H distributions are of similar shape when aligned using mean values for the populations. The similarity, however, is less good, and no negative heights exist for comparison. So, analysis is less straightforward. Furthermore, due to the likely asymmetrical distribution of errors (Fig. 11a,c), the errors spread out the input distribution but also increase heights as can be done by a scaling factor. Misfit functions from an inversion therefore contain a trade-off, not a minimum as for V. However, using the misfit surface, the following can be stated. Firstly, if errors in the recovery of height (Fig. 11 a,c) are correct, H_{in} values need to be multiplied by ~0.7 for both Methods 1 and 2 in order to achieve a best fit. Namely, input heights are overestimated by ~40%. An alternative would be to assume that heights, H_{in}, are correct and errors differ between the real and synthetic DEMs. However, running the Method 2 variant of same procedure used to estimated H_{in} on the appropriate 10 synthetic DEMs gives median H_r/H_{in} values of 1.40±0.09 (1σ), a ~20–60% height overestimation. This ~40% figure for height overestimation is valid for the procedure's treatment of idealised Gaussian shapes of a distribution not yet proven to match reality, but even this is quite strong evidence of at least some overestimation of H_{in}. This is an indicator in favour of the first case where H_{in} is overestimated and errors in recovery are similar for the real and synthetic data.

In summary, the simplest explanation for the similarity in the shapes of the recovered distributions, of H_{r} and V_{r}, is therefore that the synthetic DEMs and drumlins well represent those digitised in Smith et al. (2009), at least in regard to the application of quantification techniques. It is also demonstrated that secure conclusions can be reached, with a little further analysis to understand discrepancies if necessary, even if input populations are probably not perfect. Namely, the approach using synthetic DEMs appears robust and of practical use.

6.1 The cookie cutter method

The nature of the errors affecting the cookie cutter is qualitatively predictable, without using synthetic DEMs, by understanding the nature of the bi-cubic spline used. Consider a profile (Fig. 14). Slopes immediately outside the drumlin dictate initial trajectories immediately inside it, which the spline joins by varying gradient as smoothly as possible (e.g. Smith and Wessel, 1990). Small-scale high magnitude slopes in the measured DEM cause the interpolation on one side to descend steeply whilst the other rises. H is then overestimated: $H_r > H_{in}$. Since H is the maximum height difference, a difference $> H_{in}$ need only occur once at any point for an overestimate to occur. So, height overestimates are expected. V is the sum of over-estimated (+) and under-estimated (-) regions (shaded). So V may be high, low, accurate or even negative whilst height is positive. Overall, however, if noise creates random gradients at drumlins' boundaries, errors randomly distributed about true values (e.g. Fig. 11b) are expected. The numerical analysis is needed to build upon this qualitative understanding. Illustrative analyses presented here determine the size of errors for key derived parameters (e.g. $\overline{H}, \overline{V}$) and whether they are at all accurate. Some are not. Results derived using Methods 1 and 2 agree well (Figs. 10–13), giving confidence in such analyses. So, synthetic landscapes created with idealised landforms within a real DEM can offer valuable insights into 3D landform extraction methodologies.

6.2 Other landform quantification techniques

The analyses performed with a variant on the cookie-cutter, using an un-tensioned spine, illustrate that synthetic DEMs may also be used to compare landform quantification techniques. Tensioning a bi-cubic spline reduces the amplitude of the extremes in its extrapolation. So errors are expected to be larger for an un-tensioned spline. This is confirmed and quantified by the numerical analysis. For the 1780 individual synthetic drumlins generated using Method 1 an un-tensioned spline induces about twice (×1.79) as much error as the tensioned spline, with standard deviations of the ratio V_r/V_{in} being 1.29 and 2.29 respectively. Figures for Method 2 are 2.96 and 5.01. So, the use of a tensioned spline by Smith et al. (2009) appears justified.

6.3 Sub-populations

By linking input and recovered values for synthetic drumlins it is possible to examine claims in a depth that is not possible without synthetic DEMs. An analysis of the LGM and YD sub-populations in the study area demonstrates that it is possible to much better assess observations in the light of uncertainty in extracting drumlins' parameters. For instance, the apparently statistically significant difference in mean volume ($\Delta\overline{V}_r$) between sub-populations of different ages (Smith et al., 2009), which may reflect glacial stress patterns (e.g. Rose, 1989), is demonstrated to be only 30–50 % likely to exist in reality. Importantly, therefore, observations and scientific conclusions based upon them must remain in some doubt until errors are assessed. This assessment is significantly less practical where quantifications are done manually. Synthetic DEMs can also assess previous intractable issues such as the stationarity of the landscape with respect to the extraction of drumlins parameters. For instance, could the $\Delta\overline{V}_r$ of Smith et al. (2009) merely result from differences in the character of noise or hills in the LGM and YD areas and how this affects drumlin extraction? The analyses (Section 5.4) indicate not, which is reassuring for researchers interested in interpreting geomorphic signal and not noise. Other tests, e.g. to quantify the effect of errors in manual digitisation, are possible using the synthetic DEMs but the two done above serve to highlight the potential.

7. Conclusions

A novel way, using synthetic drumlins in a real DEM, is demonstrated to objectively test 3D landform quantification methods and probe their results in more depth than has previously been possible. Significant developments are i) the use of idealised drumlins, and ii) positioning them randomly with respect to the real noise and regional trends that cause the errors, which is the key to allowing the quality of the extraction to be assessed. Creating synthetic drumlins using height-width-length (*H*-*W*-*L*) triplets extracted from measured DEM and digitised outlines simplifies the implementation. The synthetic DEMs are demonstrably representative of the observed landscape and circularity, the retrieval of input assumptions, is avoided.

184 drumlins in Central Western Scotland, and the application of the cookie cutter technique to them (Smith et al., 2009), are used as a case study. From this, the following specific conclusions may be drawn.

Directly from the measured DEM and digitised outlines:

1. A suitable, representative 3D form of drumlins, in this area at least, is an elongated Gaussian.

Justified predominantly by the similarity in the form of *V* and *H* distributions recovered from the real and synthetic DEMs, about the proposed method:

2. Initial, somewhat naïve, methodologies to remove existing drumlins and approximate 'input' drumlin populations (*H*-*W*-*L*) re-inserted into the synthetic DEMs are sufficient, i.e. the DEMs produced include drumlins that behave in a way closely representative of the real ones during the recovery of *H* and *V*.
3. Orientations, θ, and positions (x, y) of synthetic drumlins randomly assigned, but according to observed distributions, are sufficient.
4. The Gaussian approximation does not significantly or systematically affect how drumlins are recovered.

Regarding analysis of Central Western Scotland area as in Smith et al. (2009):

5. V and H for individual drumlins are both recovered poorly.
6. Mean volume, $\overline{V}$, an important descriptive parameter for the population, is recovered well because errors in individual volume estimates are randomly distributed about the true values.
7. Mean height, $\overline{H}$, is recovered poorly as individual heights tend to be overestimated, highlighting the desirability of understanding errors.
8. Smith et al. (2009) were correct to select a tensioned, rather than an un-tensioned, spline in the cookie cutter. This choice approximately halves errors. More generally, this demonstrates the ability of synthetic DEMs to test possible quantification methods for an area.
9. If recovery errors are considered the previously observed, statistically significant (p = 0.007) difference in recovered mean volumes between Younger Dryas (YD) and Last Glacial Maximum (LGM) age sub-populations of landforms is only 30–50% likely to exist in reality. Thus, claims regarding observations thought to reflect formational, physical, Earth surface processes should be considered in light of error in the recovery of parameters.

10. Acknowledgements

The NEXTMap DEM was kindly supplied by the British Geological Survey. We thank Niels Hovius, Katrien Van Landeghem, and an anonymous reviewer for their comments, which helped improve this work. Various figures in this manuscript and geometrical computations (e.g. splines) used the GMT software package (Wessel and Smith, 1998).

11. Appendix A: Drumlin parameterisation methods

Both methods described here to parameterise drumlins are new. Initially they locate the 'core' of the drumlin (C_{xy}) then place the longitudinal (long) and transverse (short) axes. This reverses approaches such as that used by of Spagnolo et al. (2010) and is preferred here because they are consistent with how one might assess drumlins in the field or manually from a map.

A.1 Method 1: Central point

Within drumlins, in general, height of the landform (H_{drumlin}) increases as distance from the planform edge of the drumlin increases. In plan view, therefore, the core of a drumlin might be associated with a central point furthest from any edge: white circle, Fig. 3a. The smallest distance between the centre of each cell in the 5 m by 5 m grid and the outline was computed. Then the cell with the largest of these was selected as the centre, C_{xy}. This replicates one way in which a drumlin's core may be manually located on a map.

L is the length of the longest line running through C_{xy} within the drumlin. To determine L, lengths (l) of all lines starting at a digitised vertex, angle θ_l clockwise from north, were computed. Figure 6a illustrates this for an idealised drumlin. For real drumlins, the orientation of L, θ_L, is usually tightly defined (Fig. 6b, white dot), and the shortest l at about 90° to θ_L. θ_S, the angle of the transverse axis, is therefore taken to be θ_L + 90°. W is the length of this line. To prevent any possible effects of the irregular vertex density present due to manual digitisation additional vertices were placed, by linear interpolation, every 5 m along the outline.

H was calculated along the longitudinal long axis, the maximum vertical difference between the DEM after noise has been removed (Fig. 3b) and a linear interpolation between heights at the edges of the drumlin (dotted line, Fig. 4a). Height could also be defined perpendicular to the basal line, reducing it to $H\cos(\alpha)$ where α is the slope of the basal surface, but the effect is small ($\overline{\Delta H}$ = 1.47 % 2 s.f.).

Method 1 does not estimate a basal surface from the DEM. V is calculated from H, W and L (Eq. A.1). 0.253 is the constant appropriate to the idealised Gaussian shape proposed.

Eq. (A.1) $$V = 0.253 \times H \times W \times L$$

Using parameter values derived using Method 2, there is close agreement (r^2 = 0.8724, n =173) between the volumes estimated using Eq. A.1 and a grid-based calculation (Fig. 8b, grey and dashed lines), justifying this approach.

C_{xy} estimates for Method 1 are not affected by topographic clutter. Its basal estimation is simple and transparent, but depends entirely upon heights at the drumlin's outline, and is thus affected by spatial error in digitisation (Fig. 4a). Parameters derived using Method 1, however, do not depend upon the 500 m wide median filter. The profile in Fig. 4a also highlights how height within a manually digitised landform may not reflect the conventional stoss-lee form. All 178 drumlins have $H > 0$ using Method 1.

A.2 Method 2: Highest point

In the field, a drumlin's highest point can be located geographically, and might be considered to lie over its core at C_{xy}. If significant, larger scale topographic trends underlie the drumlin they should be accounted for. Accordingly, C_{xy} may be estimated in a DEM as the location of the maximum height in H_{drumlin}, the component of topography associated with drumlins. As described in Section 3.1 median filters (60 m, 500 m) have been used to define H_{drumlin}.

In Method 2 H was computed as the maximum height, and V was calculated as the volume associated with the component H_{drumlin} for the area inside the landform. Again, L and W are estimated as in Fig. 6. In Method 2, the median filters used to determine C_{xy} are not affected by digitisation errors, but the basal surface may be biased upwards (Fig. 4a) or the drumlin's upper surface distorted by incompletely eliminated topographic noise. Method 2 therefore offers a contrast to Method 1. 173 of 178 drumlins have $H > 0$ using Method 2.

A.3 Parameter populations produced

The populations of parameters calculated by the two methods are similar (Fig. 5), and differences are readily explicable. For instance, W (Fig. 5e) is larger for Method 1 because it is designed to locate the drumlin's centre as far as possible from the outline. H is greater for the results of Smith et al. (2009) than either method because its heights are affected by clutter (e.g. trees), but this is expected. Lower volumes in Method 2 than are explained by the basal surface (500 m median filter) being raised (Fig. 3a). This is typical where 'normal' terrain not containing drumlins is in a minority, especially on slopes (Wessel, 1998). Volumes recovered by the Smith et al. (2009) lie between those of Methods 1 and 2, (Fig. 5b) suggesting that conclusions about V may be safely drawn from observations seen in analyses of both methods. Dominant orientations, θ_L, indicated by steeper slopes in Figure 5a, are between 60–120° and 240–300° for both methods in good agreement with visual assessment of Figure 1c. Lastly, as expected of drumlin populations, there are more small drumlins than large ones in terms of W, L, H and V, with the caveat that the smallest W and L are scarce.

12. Appendix B: The Gaussian approximation used

Height, h_{xy} for a position (x, y) within an elongate Gaussian form centred on (x_0, y_0) of orientation θ_L (Fig. 6) is, in Cartesian coordinates, described by Eqs. B.1–8. H is the height of the drumlin.

L is length, and W is width. H_G is the full height of the Gaussian, and H_f the fraction of this used for the drumlin (e.g. 0.9 for the top 90%).

Eq. (B.1) $$h_{xy} = H_G \exp\left[-(a(x - x_0)^2 + 2b(x - x_0)(y - y_0) + c(y - y_0)^2)\right] - H_G + H$$

Eq. (B.2) $$a = \frac{\cos^2\phi}{2\sigma_L} + \frac{\sin^2\phi}{2\sigma_W}$$

Eq. (B.3) $$b = \frac{\sin 2\phi}{4\sigma_L^2} + \frac{\sin 2\phi}{4\sigma_W^2}$$

Eq. (B.4) $$c = \frac{\sin^2\phi}{2\sigma_L^2} + \frac{\cos^2\phi}{2\sigma_W^2}$$

Eq. (B.5) $$H_G = \frac{H}{H_f}$$

Eq. (B.6) $$\sigma_L = \frac{L}{\sqrt{-8\ln(1 - H_f)}}$$

Eq. (B.7) $$\sigma_W = \frac{W}{\sqrt{-8\ln(1 - H_f)}}$$

Eq. (B.8) $$\phi = \theta_L - 90$$

13. Appendix C: Synthetic DEM generation procedures

In order to approximate spatial clustering an acceptance-rejection algorithm was used (e.g. Von Neumann, 1951). Firstly, the spatial density of drumlins was computed (Fig. 9b). Trial locations (x,y) for drumlins were then generated at an even spatial density using two random numbers, but these locations were rejected if i) a third random number generated with even density in the range zero to one lay above the surface in Figure 9b or ii) the proposed drumlin footprint overlapped any existing footprints. This latter condition required that drumlins be located in order of decreasing size, otherwise 'space problems' led to larger drumlins being preferentially located in areas of lower observed drumlin density. θ values were created by a standard method; random values (0 to 1) of the cumulative probability distribution of θ (Fig. 8a) were used, each of which corresponds uniquely to a θ value. The combined cumulative θ_L distribution of 10 populations (n = 1780) is visually indistinguishable from the observed population (Fig. 8a).

gawk, using *random()* in *stdlib.h* was used to generate pseudorandom numbers. These are non-cyclic over very long periods, sufficient at least to avoid interdependencies in the ‘random’ numbers used in this study.

14. Appendix D: Stochastic modelling

The stochastic assessment used repeated random sub-division of the drumlin populations into LGM and YD sub-populations of appropriate sizes. 100,000 iterations were used to generate the probability density functions for $\Delta\overline{\ln(V_r)}$ (Fig. 10). Three such distributions were generated, one for the original data and DEM (Smith et al., 2009), and one for each of the sets of 10 synthetic DEMs related to Methods 1 and 2. For the latter, one of the 10 DEMs was selected randomly each iteration. Implicitly, such indiscriminate assignment of drumlins to sub-populations employed the null hypothesis, H_0: no difference exists. Using 100,000 iterations critical values (e.g. $\Delta\overline{\ln(V)}_{crit}$) at the 95% significance level are 5,000th in lists of generated differences (e.g. $\Delta\overline{\ln(V_r)}$) ordered in descending magnitude: These are the levels that, if exceeded, occur rarely by chance and imply a statistically significant difference. $\Delta\overline{\ln(V_r)}$ of Smith et al. (2009) is 1.38 times that of the 95% critical value of its distribution, so instances where $\Delta\overline{\ln(V_r)}$ was more that $1.38 \times \Delta\overline{\ln(V)}_{crit}$ for the synthetic DEMs were taken as more extreme than those reported by Smith et al. (2009). The similarity in the shape of the distributions that makes this test valid is evidenced visually (Fig. 10), and by similar numbers of simulations containing more extreme differences than the threshold: 715 for the data of Smith et al. (2009), and 628 and 750 for Methods 1 and 2 respectively. Methods 1 and 2 use 178 and 173 drumlins respectively, bracketing the n = 175 of Smith et al. (2009). Agreement between the methods, therefore, indicates insensitivity to these variations. Consequently, no correction was made for the difference in n.

References

Amundson, J. M., Iverson, N. R., 2006. Testing a glacial erosion rule using hang heights of hanging valleys, Jasper National Park, Alberta, Canada. J. Geophys. Res. Earth Surface 111, art. no. F01020.

Braun, J., Sambridge, M, 1997. Modelling landscape evolution on geological time scales: A new method based on irregular spatial discretization. Basin Research 9, 27-52.

Brocklehurst, S. H., Wipple, K. X., 2004. Hypsometry of glaciated landscapes. Earth Surface Processes and Landforms 29, 907-926.

Chase, C. G., 1992. Fluvial landscupting and the fractal dimension of topography. Geomorphology 5, 39-57.

Cheng, Q. M., Agterberg, F. P., 1996. Multi-fractal modelling and spatial statistics Mathematical Geology 28, 1-16.

Chorley, R. J., 1959. The Shape of Drumlins. J. Glaciol. 3, 339-344.

Clark, C., Hughes A., Greenwood, S., Spagnolo, M., Ng, F., 2009. Size and shape characteristics of drumlins, derived from a large sample, and their associated scaling laws. Quart. Sci. Rev. 28, 677-692.

Densmore, A. L., Ellis, M. A., Anderson, R. S., 1998. Landsliding and the evolution of normal-fault-bounded mountains. J. Geophys. Res. 103(B7), 15203-15219. doi:10.1029/98JB00510

Dziewonski, A., Hager, B., O'Connell, R., 1977. Large-scale heterogeneities in the lower mantle. J. Geophys. Res. 82, 239-255.

Evans, I. C., 1987. A new approach to drumlin morphometry p119-130. In: J. Menzies and J. Rose (Eds.), Drumlin Symposium. Balkema, Rotterdam.

Fowler, A. C., 2000. An instability mechanism for drumlin formation p307-319 In Deformation of Glacial Materials (Ed. Maltman, A. J.) Geol. Soc. Sepcial Publication 176.

Fowler, A. C., 2009. Instability modelling of drumlin formation incorporating lee-side cavity growth. Proc. R. Soc A 465, 2681-2702.

Fowler, A. C., 2010a. The instability theory of drumlin formation applied to Newtonian viscous ice of finite depth Proc. R. Soc. A 466, 2673-2694.

Fowler, A. C., 2010b. The formation of subglacial streams and mega-scale glacial lineations Proc. R. Soc. A 466, 3181-3201.

Gagnon, J. S., Lovejoy, S., Schertzer, D., 2006. Multifractal Earth topography Nonlinear Processes in Geophysics 5, 541-570.

Gilbert L. E., 1989. Are topographic data sets fractal? Pure and Applied Geophysics 131, 241-254.

Harbour, J. M., 1992. Numerical Modeling of the development of U-shaped valleys by glacial erosion. Geol. Soc. Am. Bull. 104, 1364-1375.

Hillier, J. K., Watts, A. B, 2004. “Plate-like" subsidence of the East Pacific Rise - South Pacific Superswell System J. Geophys. Res. 109, B10102 doi 10.1029/2004JB003041.

Hillier, J. K., 2008. Seamount detection and isolation with a modified wavelet transform Basin Research 20, 555-573.

Hillier, J. K., Smith, M., 2008. Residual relief separation: digital elevation model enhancement for geomorphological mapping. Earth Surface Processes and Landforms 33, 2266-2276 doi: 10.1002/esp.1659

Hindmarsh, R. C. A., 1998. Drumlinization and drumlin-forming instabilities: viscous till mechanisms. J. Glaciology 44, 293-314.

Hollingsworth, S. E., 1931. The glaciation of western Edenside and adjoining areas and the drumlins of Edenside and the Solway Basin Quart. Journal Geol. Soc. London 87, 281-359.

Intermap (2004) Intermap product handbook and quickstart guide (v3.3).

Jamieson, S. S. R., Hulton, N. R. J., Hagdorn, M., 2008. Modelling landscape evolution under ice sheets. Geomorphology 97 91-108

Jordan, T. A., Watts, A. B., 2005. Gravity anomalies, flexure and the elastic thickness structure of the India-Eurasia collisional system. Earth Planet. Sci. Lett. 236, 732-750.

Kim, S. and Wessel. P., 2008. Directional median filtering for the regional-residual separation of bathymetry. G3 9, Q03005 10.1029/2007GC001850

Lane, N. F., Watts, A. B., and Farrant, A. R, 2008. An analysis of Cotswold topography: insights into the landscape response to denudational isostasy. J. Geol. Soc. 165, 85-103.

Lombardini, F., 2005. Analysis of non-Gaussian speckle statistics in high-resolution SAR images IGARSS 2005: IEEE International Geoscience and Remote Sensing Symposium, Vols 1-8, Proceedings 1337-1340

Malinverno, A., 1989. Testing linear models of seafloor topography Pure and Applied Geohpysics 131, 139-155.

Mandelbrot, B., 1983. The Fractal Geometry Of Nature W. H. Freeman and Company, New York.

Marova, N. A., 2002. Seamounts of the world ocean. Oceanology, 42(3), 409 – 413.

Nolet, G., Allen, R., Zhao, Dapeng, 2007. Mantle plume tomography Chemical Geology 241, 248-263

Perron, J. T., Kirchner, J.W., Dietrich, W.E., 2008. Spectral signatures of characteristic spatial scales and nonfractal structure of landscapes J. Geophys. Res. 113, F04003.

Reed, B., Galvin, C. J., Millier, J. P., 1962. Some aspects of drumlin geometry Am. J. Sci 260, 200-210.

Rose, J., 1987. Drumlins as part of a glacier bedform continuum. 103-116 in Menzies, J., Rose. J. (Eds.) Drumlin Symposium. Balkema, Rotterdam.

Rose, J., 1989. Glacial stress patterns and sediment transfer associated with the formation of superimposed flutes. Sedimentary Geology 62, 151-176.

Rose, J., Smith, M.J., 2008. Glacial geomorphological maps of the Glasgow region, western central Scotland. Journal of Maps v2008 doi:10.4113/jom.2008.1040

Saygin, E., Kennett, B. L. N., 2010. Ambient seismic noise tomography of Australian continent. Tectonophysics 481, 116-125.

Schoof, 2007. Cavitation in deformable glacier beds. J. Appl. Math. 67, 163-1653.

Shaw, J., 1983. Drumlins formation related to inverted meltwater erosional marks. J. Glaciol. 29, 461-479.

Sissons, J. B., 1967. The Evolution of Scotland's Scenery. Oliver and Boyd, Edinburgh. pp259 ISBN 0 416 84000 0.

Sithole, G., Vosselman, G., 2004. Experimental comparison of filter algorithms for bare-Earth extraction from airborne laser scanning point coulds ISPRS. Journal of Photogrammetry and Remote Sensing 59, 85-101

Smith, M. J., Clark, C., 2005. Methods for the visualisation of digital elevation models for landform mapping. Earth Surface Processes and Landforms 30, 885-900

Smith, M. J., Wise, S. M., 2007. Mapping glacial lineaments from satellite imagery: an assessment of the problems and development of best procedure. Int. J. Applied Earth Observation and Geoinformation 9, 65-78.

Smith, M. J., Rose, J., Booth, S., 2006. Geomorphological mapping of glacial landforms from remotely sensed data: an evaluation of the principal data sources and an assessment of their quality. Geomorphology 76, 148-165.

Smith, M. J., Rose, J., Gousie, M. B., 2009. The Cookie Cutter: A method for obtaining a quantitative 3D description of glacial bedforms. Geomorphology 108, 209-218.

Smith, W., Wessel, P., 1990. Gridding With Continuous Curvature Splines in Tension. Geophysics 55, 293-305.

Spagnolo, M., Clark, C. D., Hughes, A. L. C., Dunlop, P., Stokes, C., 2010. The planar shape of drumlins. Sedimentary Geology 232, 119-131.

Sun, X., Rosin, P. L., Martin, R. M., Langbein, F. C., 2009. Noise analysis and synthesis for 3D laser depth scanners. Graphical Models 71, 34-48.

Tate N. J., 1998. Estimating the fractal dimension of synthetic topographic surfaces. Computers and Geosciences 24, 325-334.

Tate, N. J., 1998. Maximum entropy spectral analysis for the estimation of fractals in topography. Earth Surface Processes and Landforms 23, 1197-1217.

Tomkin, J. H., 2009. Numerically simulating alpine landscapes: The geomorphological consequences of incorporating glacial erosion in surface process models. Geomorphology 103, 180-188.

Tucker, G., Hancock, G. R., 2010. Modelling landscape evolution. Earth Surface Processes and Landforms 35, 28-50.

Von Neumann, J, 1951. Various techniques used in connection with random digits. Monte Carlo Methods. Nat. Bureau Standards 12, 36-38.

Weissel, J. K., Pratson, L. F., Malinverno, A., 1994. The length-scaling properties of topography. J. Geophys. Res. 99, 13997-14012.

Wessel, P., 1997. Sizes and Ages of Seamounts Using Remote Sensing: Implications for Intraplate Volcanism. Science 277, 802-805.

Wessel, P., 1998. An Empirical Method for Optimal Robust Regional-Residual Separation of Geophysical Data. Mathematical Geology 30, 391-408.

Wessel, P., and Smith W. H. F., 1998. New, improved version of Generic Mapping Tools released, EOS Trans. Amer. Geophys. U. 79(47), 579.

Wren, E. A., 1973. Trend Surface Analysis – A review. Canadian Journal of Exploration Geophysics 9(1), 39-45.

Zhou, Q. M. and Lis, X. J., 2004. Analysis of errors of derived slope an aspect related to DEM data properties. Computers and Geosciences 30, 369-378.

Figures

Figure 1: Idealised profiles to illustrate the process used to create synthetic DEMs. There are three 'components' (Hillier and Smith, 2008): Drumlins (dark grey shade) sit upon a regional trend (dotted line). Both are overlain by 'clutter' or 'noise' (light grey shade). a) Upper and lower surfaces of drumlin are estimated to define it, and it is removed (height subtracted). b) Two Gaussian shaped drumlins are inserted (height added). Noise as Fig. 4a.

Figure 2: Location maps. a) Study area is located at (4°28' W, 56°02' N), white circle: England (E), Scotland (S), Ireland (I). Coastlines of seas and major inland water bodies are shown. b) DEM of a sub-region of the study area, with height displayed as greyscale, located in c): Woodland (W), Tree (T). c) Study area, with main geomorphic features of interest highlighted; drumlins (black outlines), rivers (grey), water (grey shade). A division between Younger Dryas (YD) and Last Glacial Maximum (LGM), white and stippled areas respectively, is also shown (Smith et al., 2006). Arrows indicate approximate ice flow trends in the LGM (Sissons, 1967) and YD (Rose, 1987). Map coordinates for b) and c) are of the British National Grid. 5 m grid.

Figure 3: Example of an inspection used to assess the ability of widths of median filter to separate noise, drumlins, and hills. Also, a drumlin illustrating the estimation of parameters (x,y,L,W,θ), and selection of primary axes, from its digitized outline. a) Centre of drumlin (bold line) is at x,y (white circle), determined by Method 1. Digitized outlines of other drumlins (thin lines) overlay the measured DEM. b) Computed axes (lines) overlie 'decluttered' topography to which a 60 m wide median filter has been applied. Arrows indicate directions of increasing distance along profiles in Figure 4. c) 'Clutter' removed i.e. difference between a) and b). d) H_{hills} estimated using a 500 m median filter. Map coordinates are of the British National Grid.

Figure 4: Height profiles across drumlin in Fig. 3. Profiles start *from* the directions θ_L and θ_S such that, assuming a conventional stoss-lee form, traditional interpretations of ice flow are as indicted. Lines are: measured height (thin lines), estimates of the decluttered surface using 60 m wide median filter (thick black lines), linear interpolation between heights at the digitized edges of the drumlin (dotted lines), 500 m wide median filter (grey lines). Grey boxes delimit the drumlins. a) and b) are heights along the long and short axes, and c) and d) are normalized profiles along the same axes.

Figure 5: Stacked (i.e. average) de-trended and normalized height profiles (black lines). Dashed lines are $\pm 1\sigma$ of height and dotted lines are ±2 standard errors of the individual profiles when binned in 0.01 intervals of distance. Thick grey lines are Gaussian curves centred upon $x = 0.5$. Grey box is the bounding box for all drumlins. a) and b) are respectively for long and short axes found using Method 1, whilst c) and d) are for Method 2. All profiles start *from* the directions θ_L and θ_S. a) and b) $n = 178$, c) and d) $n = 173$.

Figure 6: Method of estimating parameters (L, W, θ_L, θ_s) after C_{xy} has been determined. a) Idealised drumlin consisting of interpolation (black line) between digitized points (black dots), with the centre C_{xy} (open circle). At each point on the outline, θ and l are calculated. b) θ and l for all points on drumlin #15 in Figure 2. θ_L (open circle) is θ for the largest l *i.e.* L, and $\theta_s = \theta_L + 90°$ (cross): Compare to θ for the smallest L (filled black circle). 'Ice flow' arrow indicates a traditional interpretation of a conventional stoss-lee form.

Figure 7: Illustrative synthetic drumlin. a) Profile across the centre of drumlin. Drumlin interior (grey shade) and topography (solid line), are the top 90% of a Gaussian curve (dashed line). b) Plan view, grey shaded relief of drumlin, where black is zero. White line locates profile in a), and dark lines trending N-S and E-W are given for reference.

Figure 8: Cumulative distributions (cdfs) of parameters (θ_L, *V, H, L*, *W*). a) Orientation: Solid black line is input values for the synthetics measured from non-Gaussian outlines in the real DEM using Method 1 (n = 178 of $H > 0$). This is overlain, indistinguishably, by the curve combining the 10 synthetic DEMs generated from this input. Grey lines are for the individual synthetic DEMs, and vertical bars are $\bar{y} \pm 2\sigma$ of the mean. Dashed line is Method 2 (n = 173 of $H > 0$). b) and c) Volume and height: Solid black and black dashed lines as a), with black dotted lines for the data of Smith et al. (2009). Dashed and dotted grey lines are values recovered by the cookie cutter from synthetic DEMs created using Method 1 and 2 respectively, although they mainly underlie the curves of the inputs in b). In b) solid grey line is an estimate of *H, W* and *L* using Method 2, which is converted to *V* using an idealised Gaussian geometry. d) and e) are distributions for length and width, with lines as in a). For consistency with the data of Smith et al. (2009) only $V > 0$ are used throughout this figure. Smith et al. (2009) do not determine θ_L, *L*, *W* for comparison.

Figure 9: Spatial distribution of drumlins. a) Observed distribution. b) Spatial density (i.e. % of area) covered by drumlin, smoothed with a three kilometre wide boxcar filter, and displayed as a proportion of the highest density within the area. c) Illustrative spatial distribution from one of 20 synthetic DEMs in study. d) Four synthetic DEMs neighbouring c) in generation process to illustrate variability. Map coordinates are of the British National Grid.

Figure 10: Visualisation of method used to assess claims about differences in mean volume between sub-populations. Probability density curves generated by stochastic analysis, n = 100,000, for the observations of Smith et al. (2009) (dotted line), Method 1 (solid line), and Method 2 (dashed line). Vertical bars are 95% critical value and the difference observed by

Smith et al. (2009). For simplicity, curves are scaled so that 95% critical values align with that generated by the data of Smith et al. (2009).

Figure 11: Effectiveness of the extraction of drumlin H and V. a) Histogram of individual height recoveries, expressed as ratio of recovered height over input height, by Method 1. Arrow is correct recovery. Circle is mean ratio, bar indicated ±1σ. Grey bars represent all drumlins, and black bars represent only large ($L > 500$ m) drumlins. b) as a) for V. c) and d) are as for a) and b) for Method 2.

Figure 12: Reliability of recovered population parameters $\overline{H}$ and $\overline{V}$ for $n = 173$. a) $\overline{H}$ for Method 1. Input mean height (light grey bar) is significantly less than recoveries from the 10 synthetic DEMs (grey dots), whose mean and range (±2σ) is displayed by the black dot and bar. b) as a), except about $\overline{V}$ and shows recoveries consistent with input values. c) and d) are as for a) and b), but for Method 2.

Figure 13: Comparison of recovered V distributions. a) Distributions recovered as Smith et al. (2009) (dotted line), and using idealised Gaussian drumlins from synthetic DEMs generated from Methods 1 and 2 (solid and dashed lines respectively). Means of the curves, $\overline{V}_r$ (solid vertical line), are aligned to that of the extraction as Smith et al. (2009) by linear multipliers applied: 'scale factor'. c) Corresponding input distributions. Grey lines are for extractions of DEMs created by Method 1 with errors of 1.0, 2.0, 3.0, 4.0 and 5.0 times those actually recovered, 'error multiplier': higher factors are lighter. b) and d) mean absolute misfit (i.e. form $\sum |x_1 - x_2|$) between curves for varied 'Scale Factor' and 'Error Multiplier' and the recoveries as Smith et al. (2009). Best fit is white circle. Contour 25% higher than the best fit defines error ellipse (black line). Search increments 0.02.

Figure 14: Schematic illustration of this action of a bi-cubic spline. Topography (solid lines) is from Fig. 1, including observed noise from Fig. 4a. Arrows indicate gradients at the outline, and dashed line is a minimum curvature (bi-cubic) interpolation (T = 0) to estimate the basal surface (dotted line). Tensioning the spline reduces the amplitude of deviations.

Tables

Table 1: Percentage of 'good' estimates, with recovered values of H and V within ±25% of actual values. Values in brackets use a variant of the cookie cutter recovery method using an un-tensioned spline.

Method	**% of** V_r/V_{in}	**% of** H_r/H_{in}
1	39.2 [26.5]	20.5 [18.6]
2	47.6 [34.3]	25.8 [23.0]

Table 2: Input and recovered population parameters. The mean and standard deviation (σ) of the estimates of $\overline{V}_r$ and $\overline{H}_r$ from 10 synthetic DEMs is reported in each case. Individual data plotted on Fig. 12, grey dots. Note, σ is not a standard error. Values in brackets use a variant of the cookie cutter recovery method using an un-tensioned spline.

Method	$\overline{V}_{in}$ (m^3)	$\overline{V}_r$ (m^3)	$\overline{H}_{in}$ (m)	$\overline{H}_r$ (m)
1	159,076	156,559 ± 8,212 (1σ) [149,255 ± 15,592]	6.82	12.54 ± 0.28 (1σ) [13.15 ± 0.26]
2	117,376	109,623 ± 4,019 (1σ) [107,717 ± 6,419]	6.43	11.76 ± 0.23 (1σ) [12.23 ± 0.24]

Table 3: Spatial effects upon extraction methodology, E_V, evaluated by comparing the difference between input and recovered values in the LGM and YD populations. Subscripts denote volume and height. Note that the standard deviation of E, σ, is the standard error of the differences between LGM and YD for individual DEMs. Square brackets are for the un-tensioned spline variant.

Method	E_V (m^3)	E_H (m)
1	1,828 ± 5,146 (1σ) [6,272 ± 5,756]	1.34 ± 0.22 (1σ) [1.28 ± 0.23]
2	-5,094 ± 2,862 (1σ) [1,033 ± 4,566]	1.15 ± 0.32 (1σ) [1.41 ± 0.39]

Figure 1

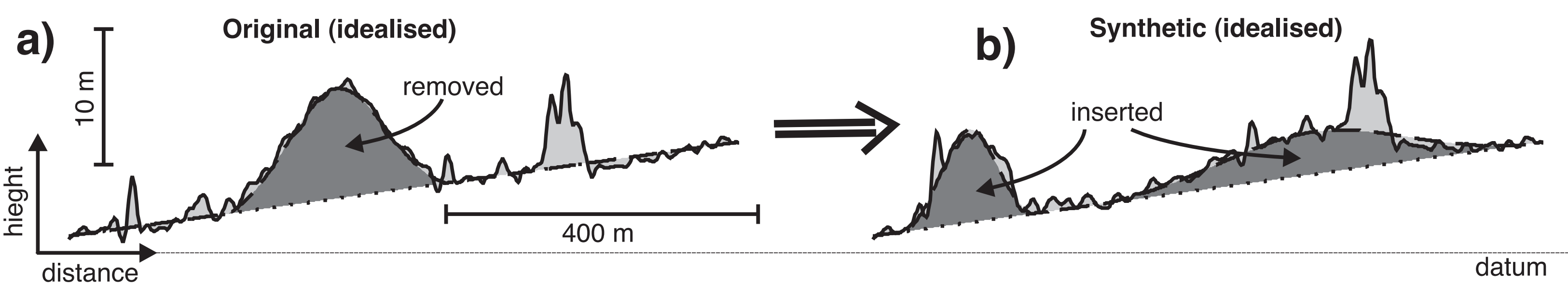

FIG 1

Figure 2

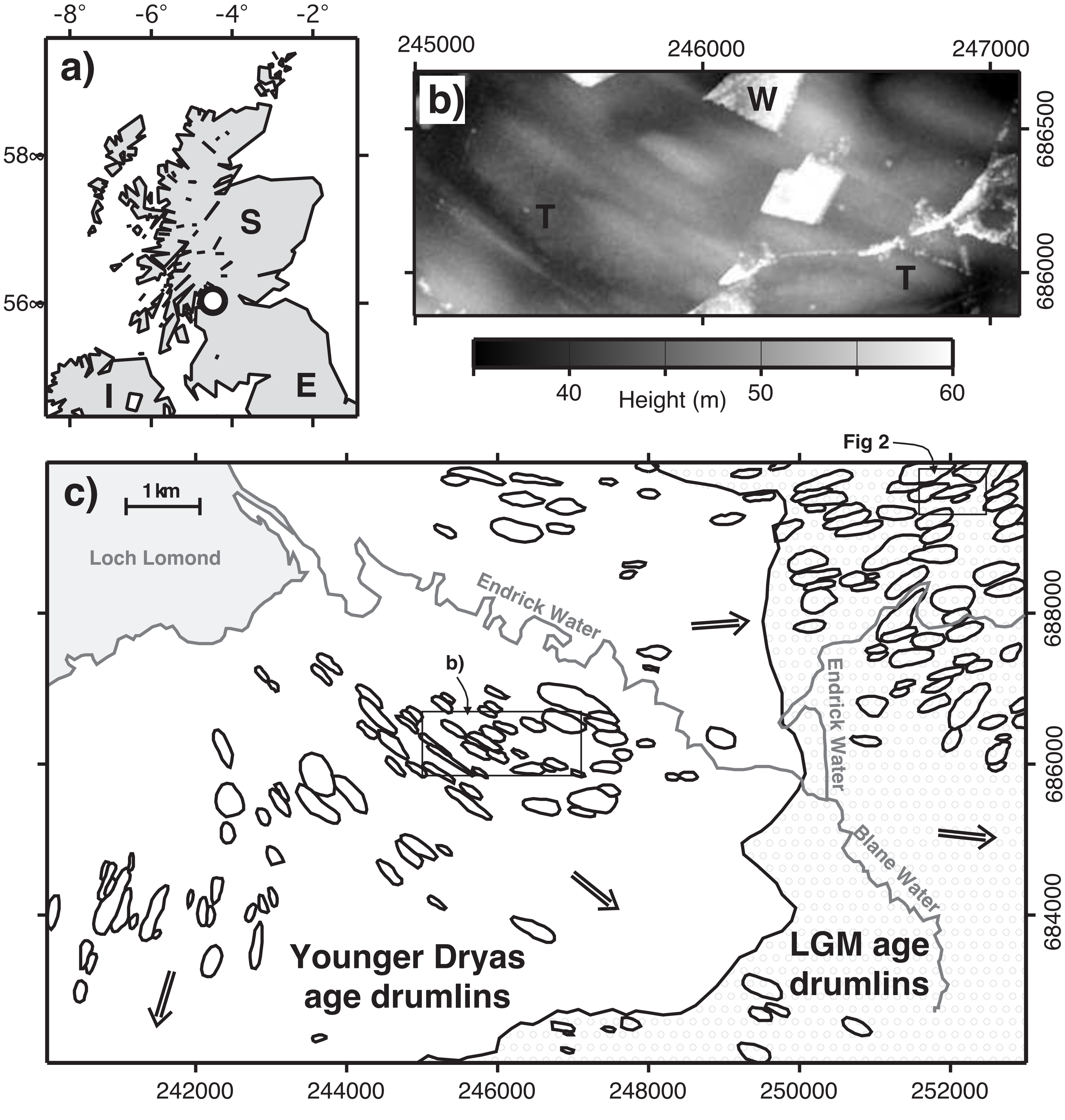

FIG 2

Figure 3

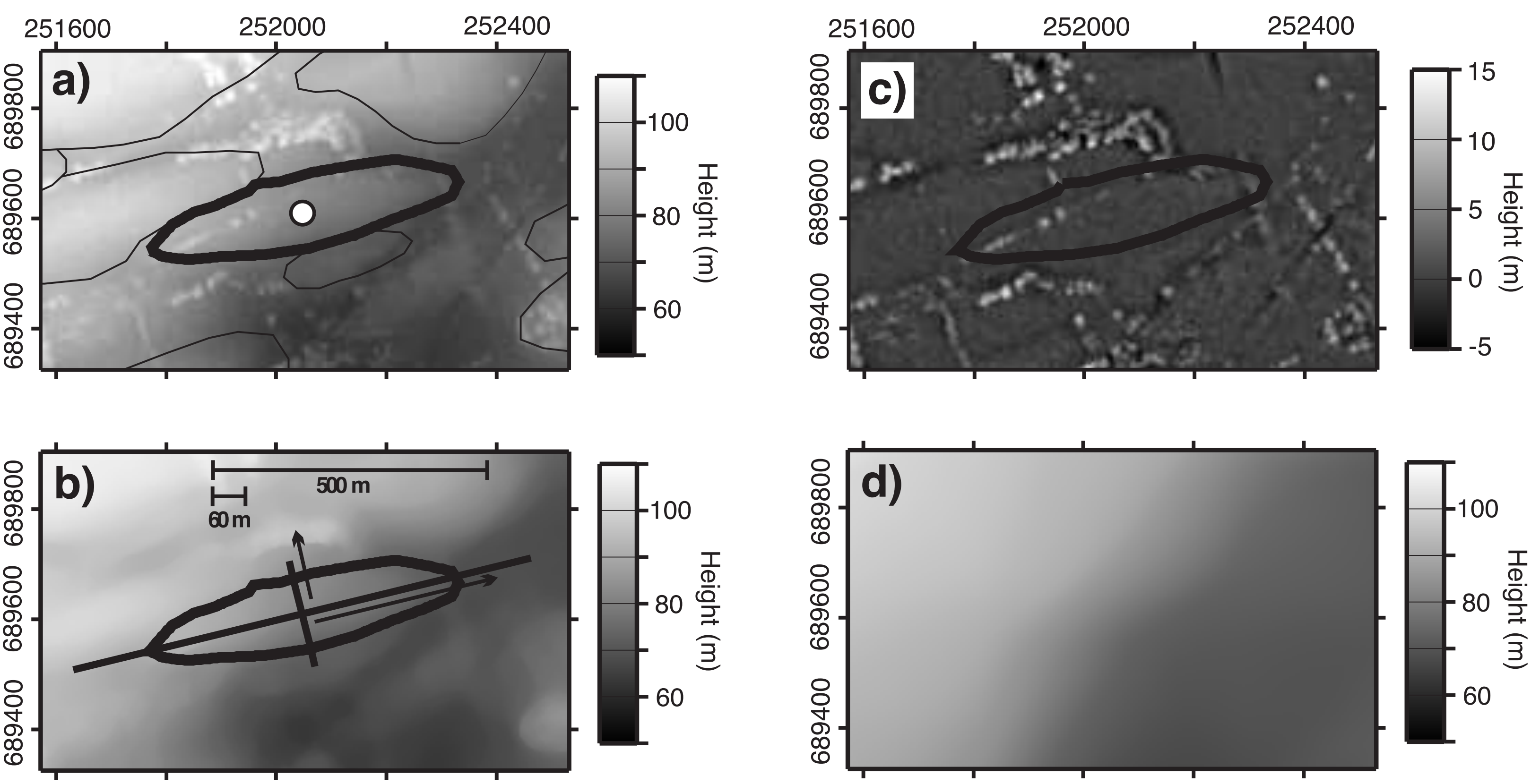

FIG 3

Figure 4

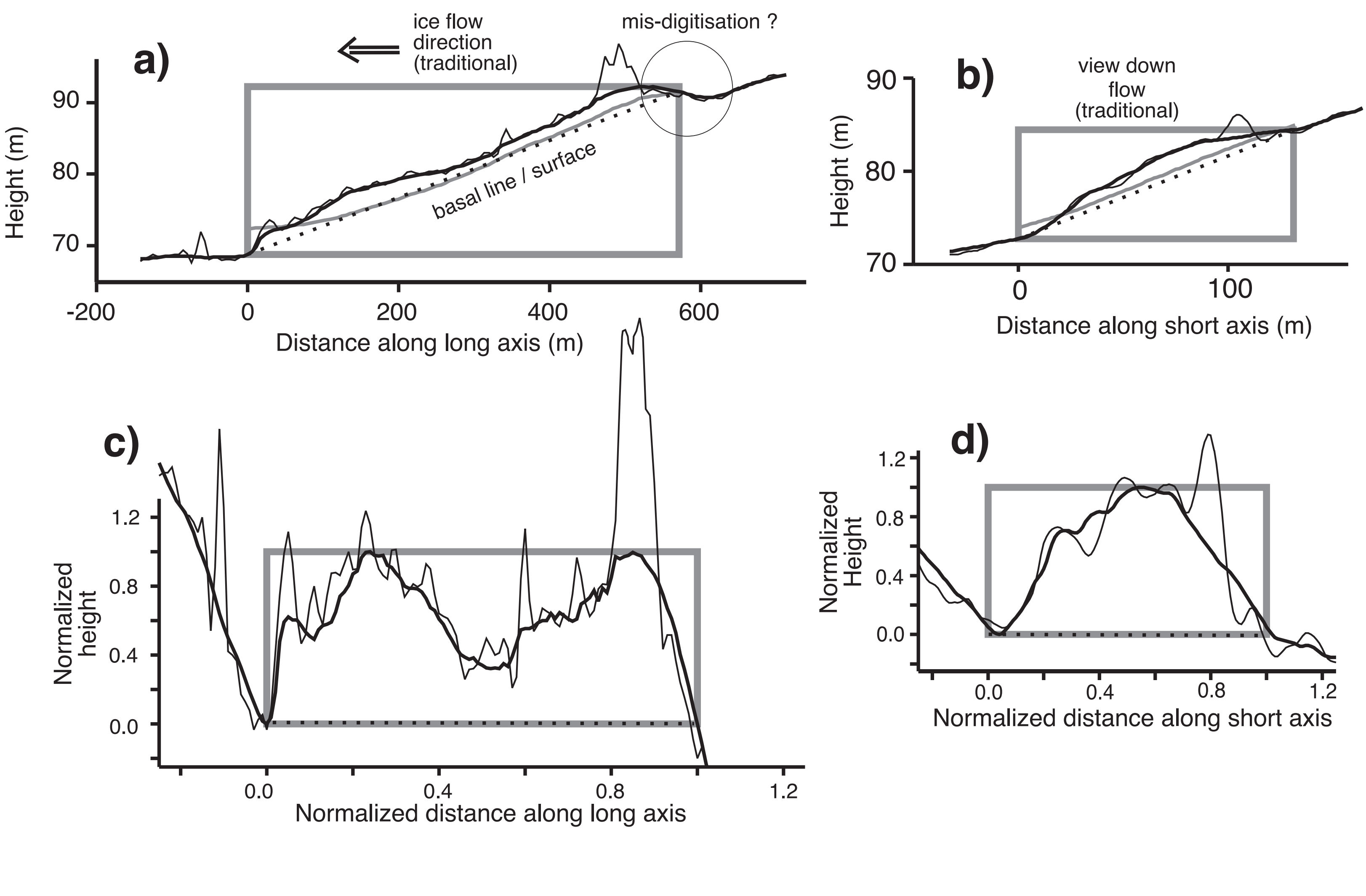

FIG 4

Figure 5

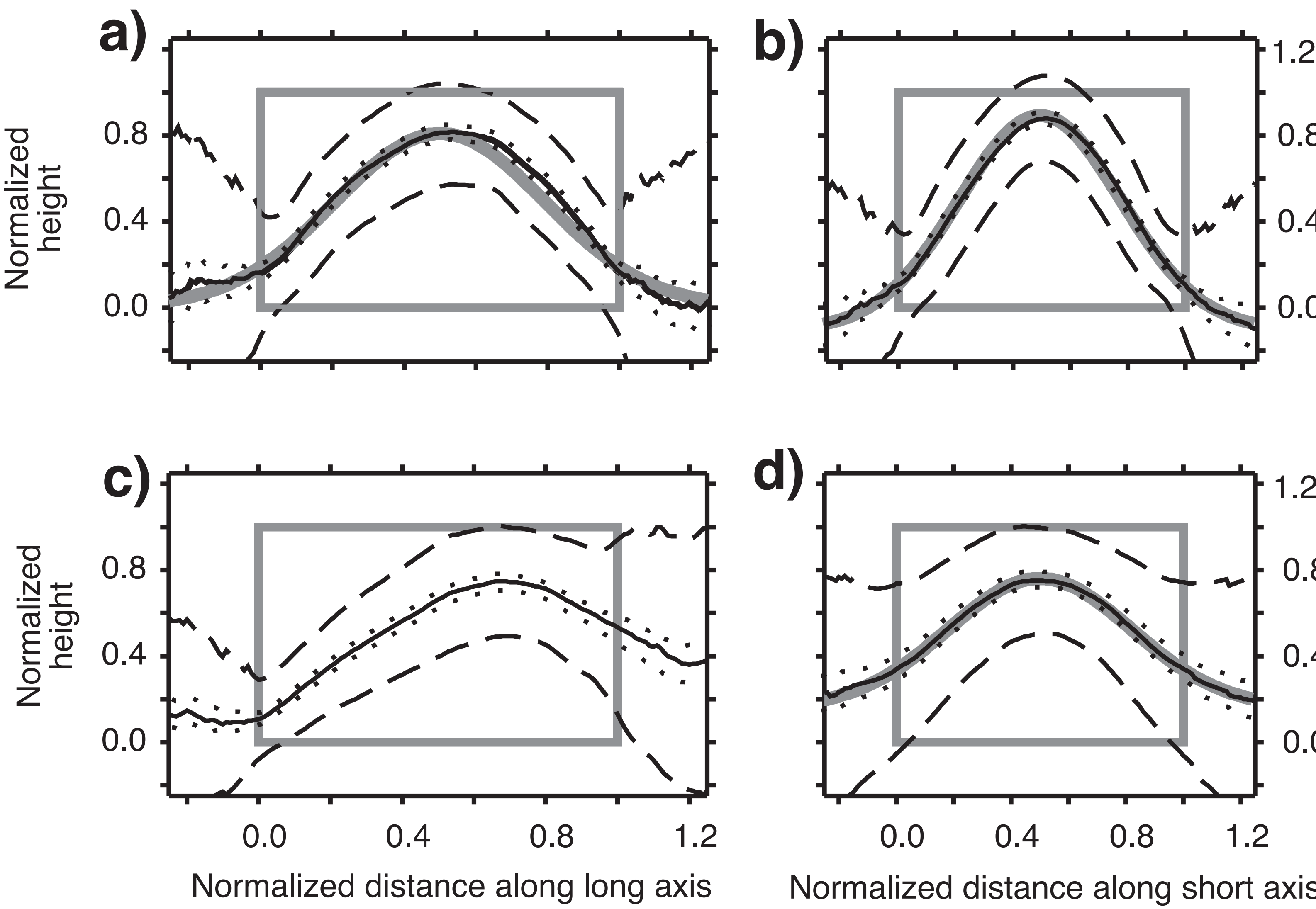

FIG 5

Figure 6

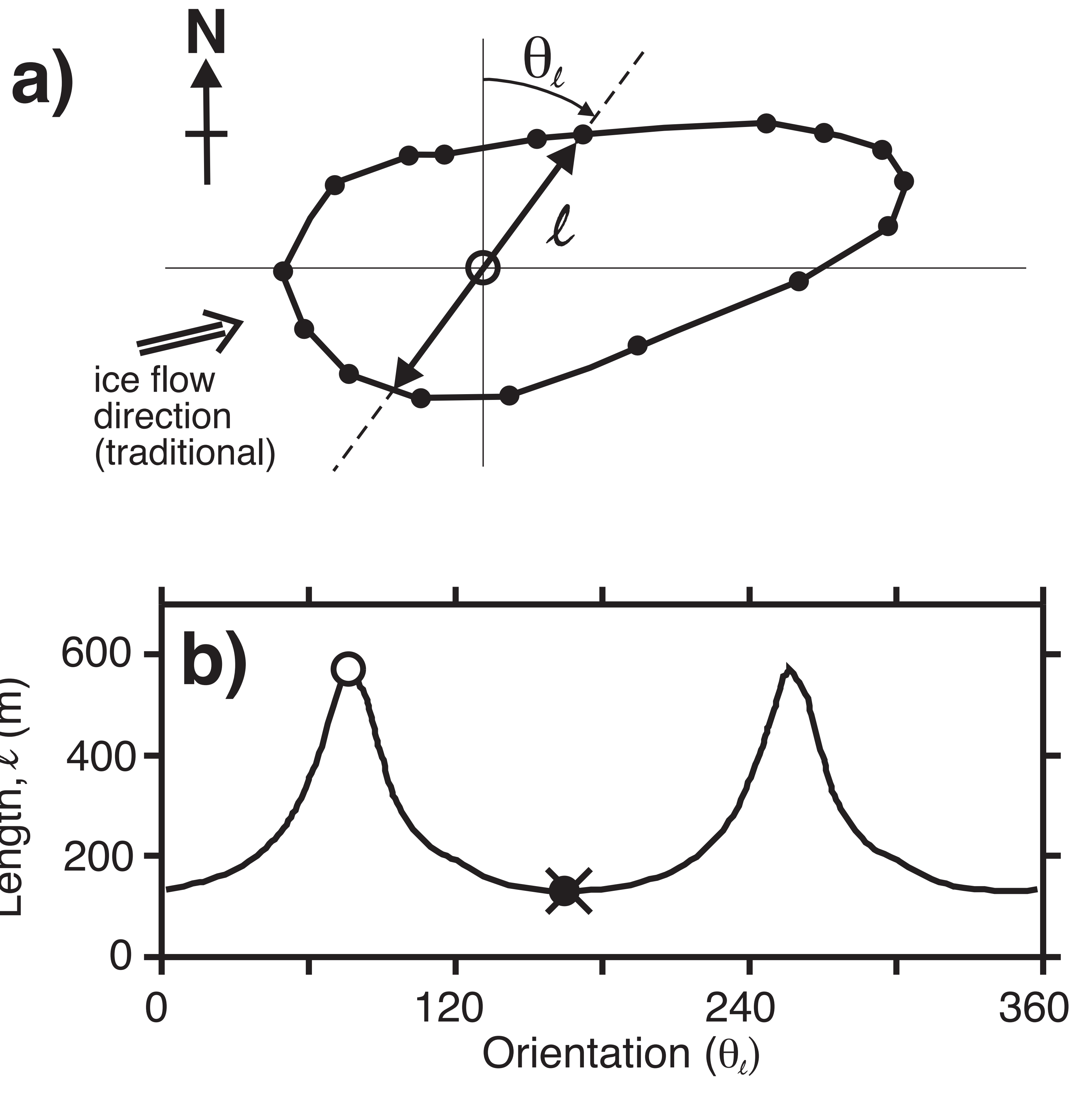

FIG 6

Figure 7
Click here to download high resolution image

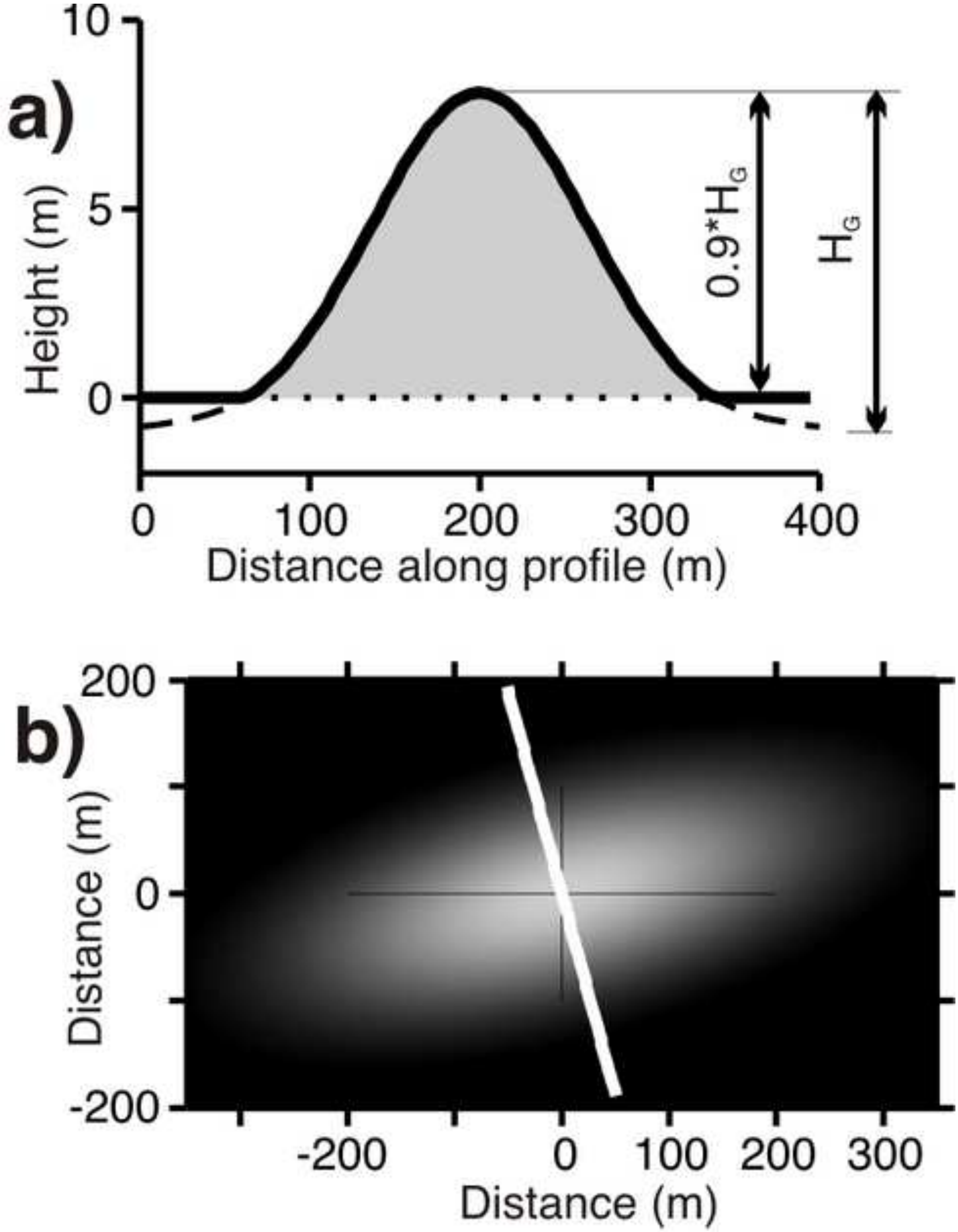

FIG 7

Figure 8

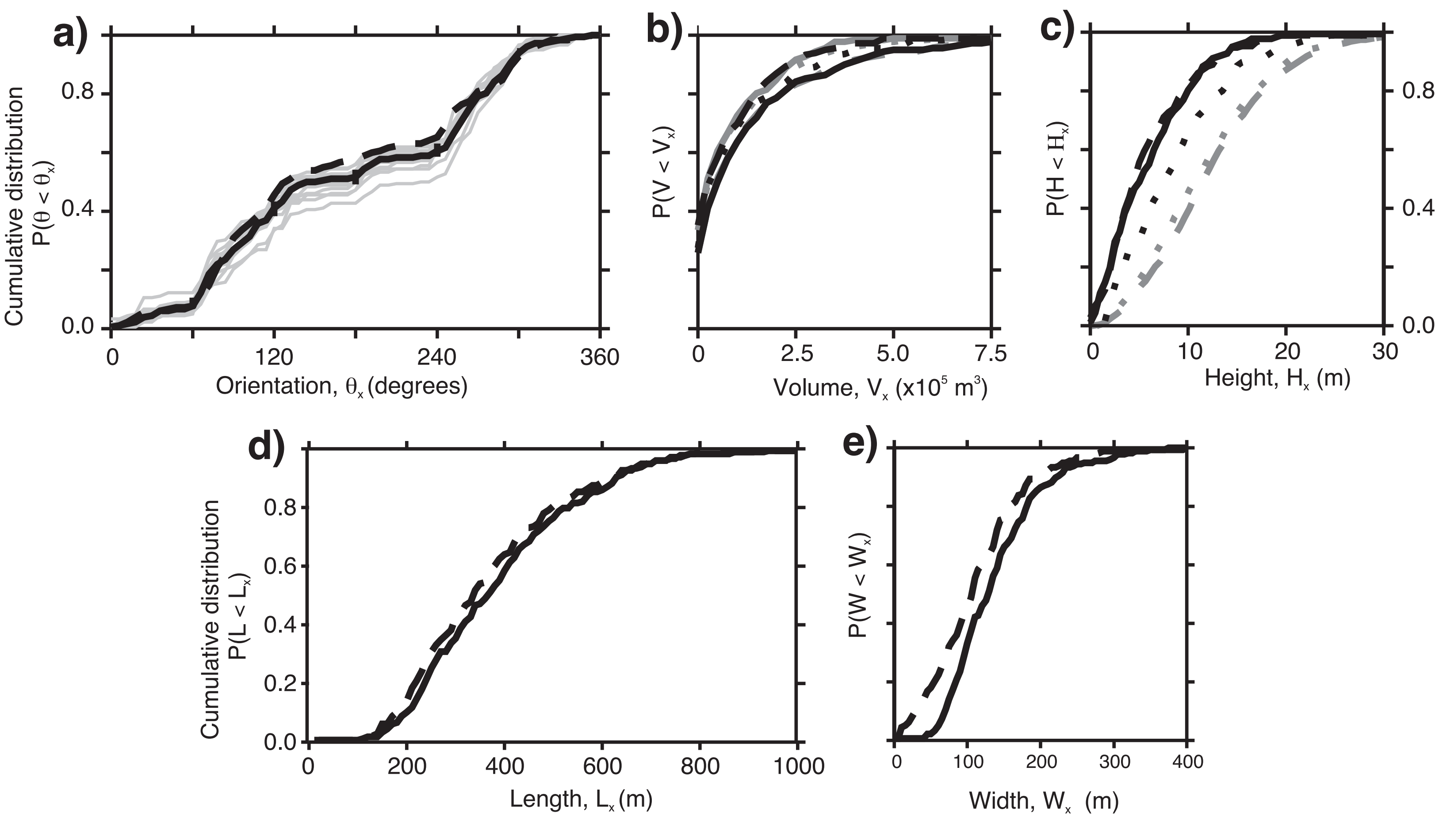

FIG 8

Figure 9

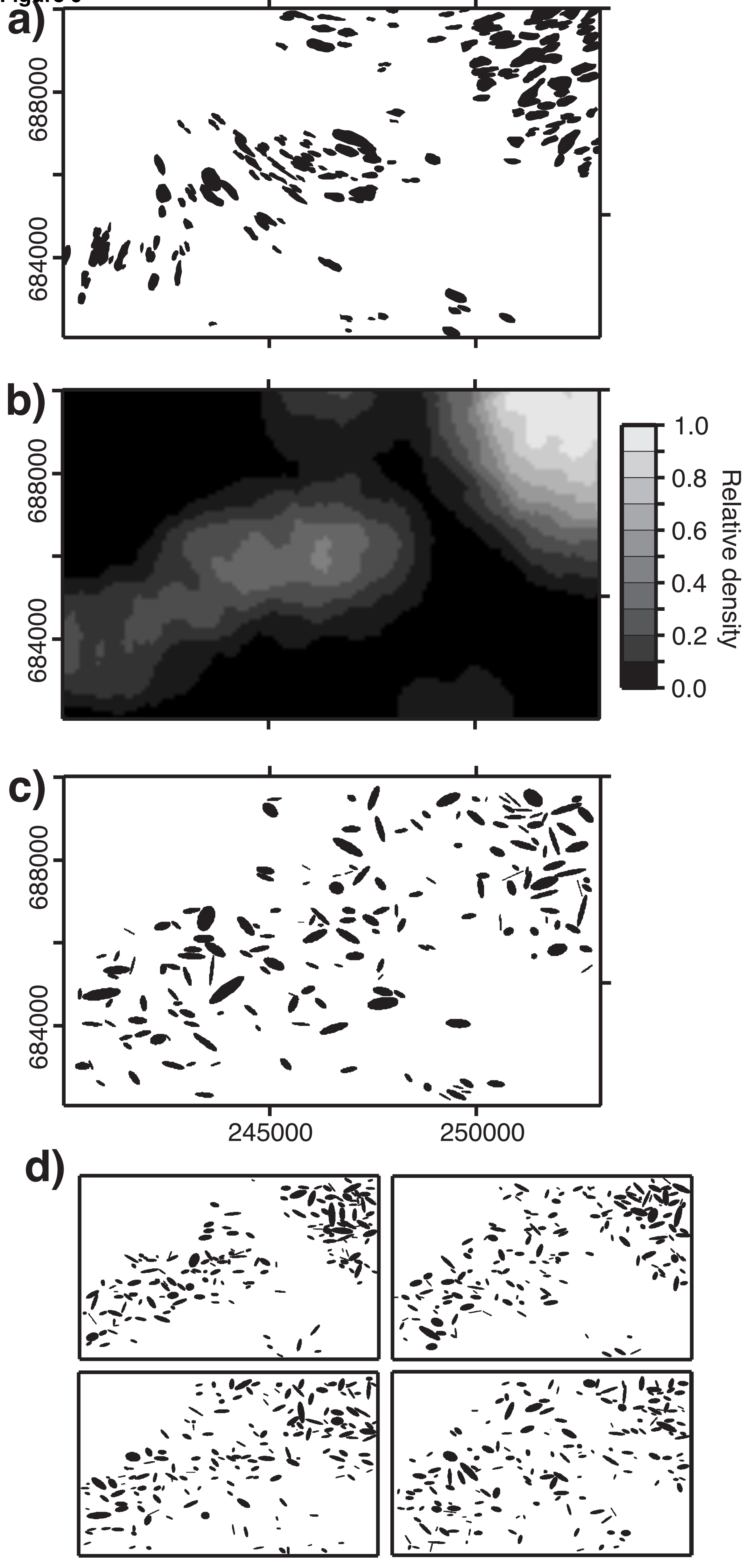

FIG 9

Figure 10

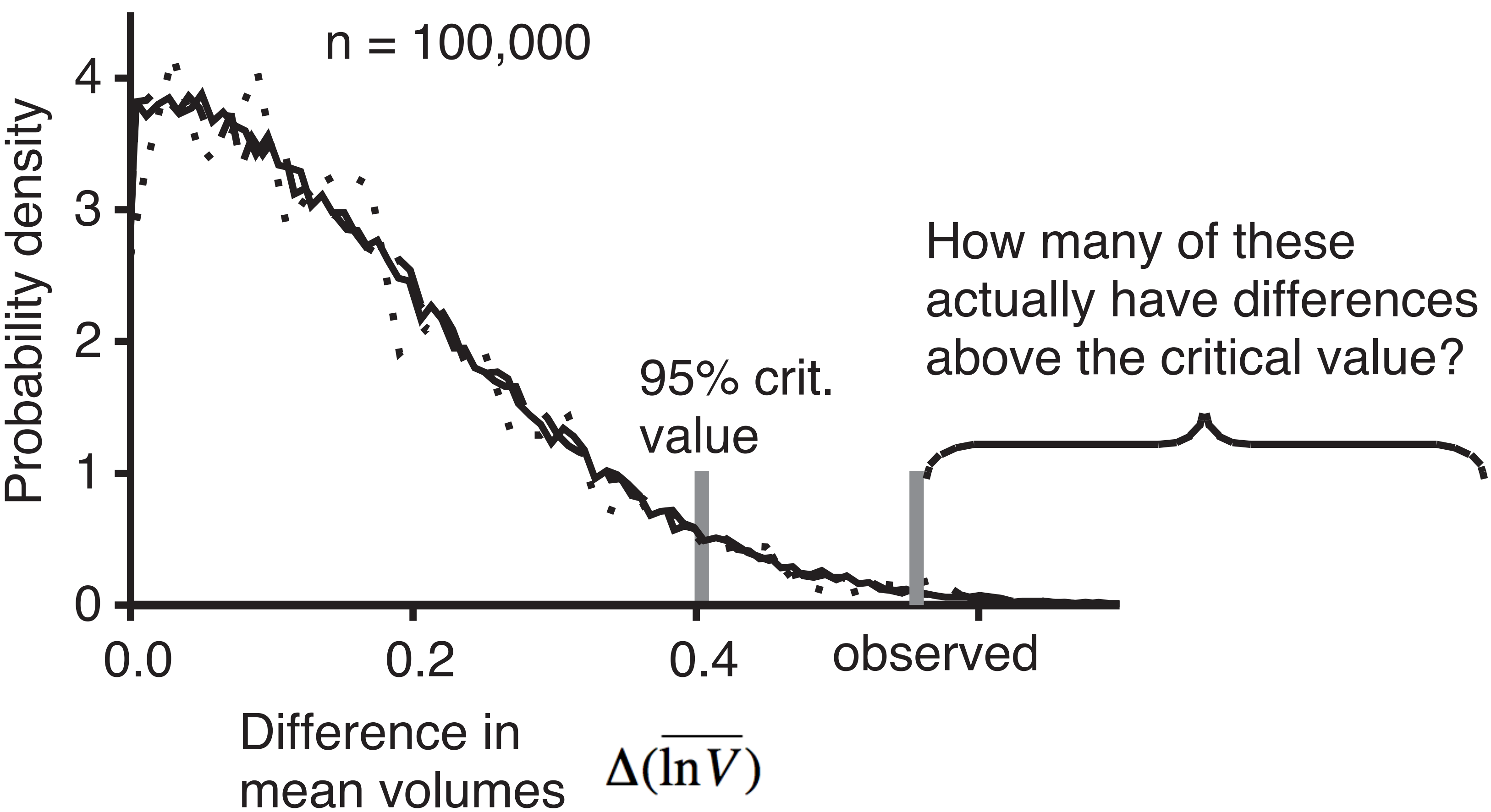

FIG 10

Figure 11

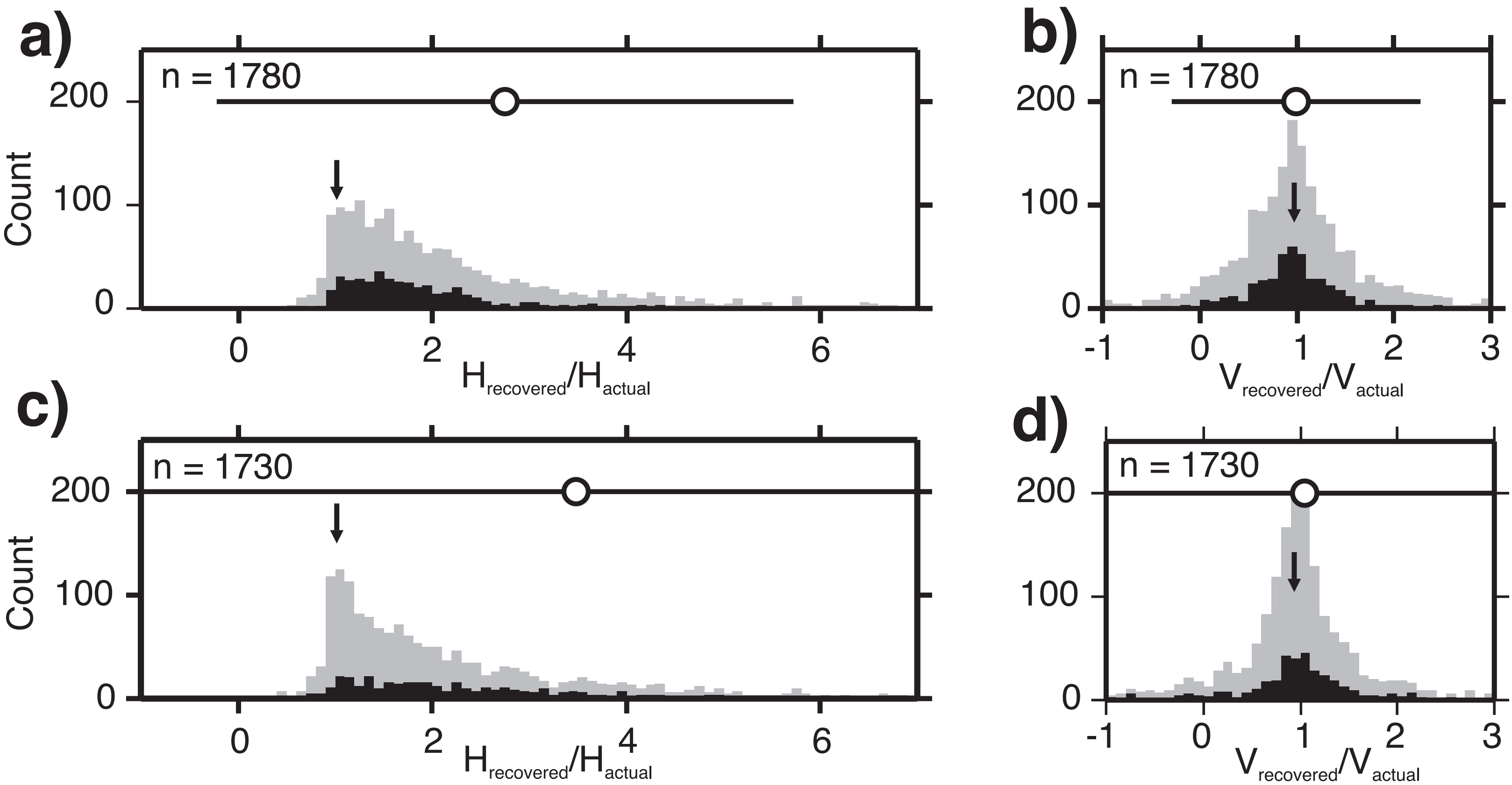

FIG 11

Figure 12

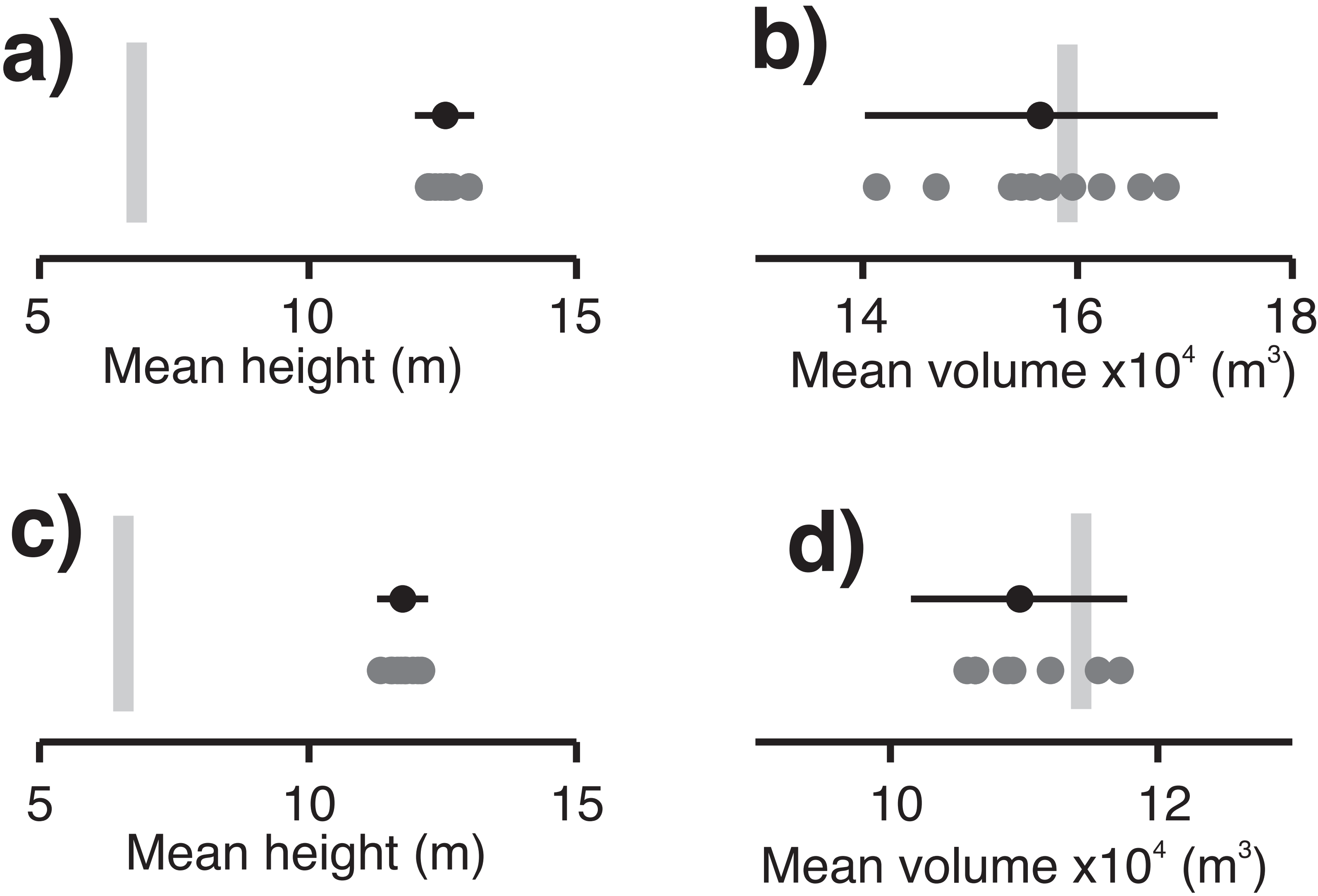

FIG 12

Figure 13

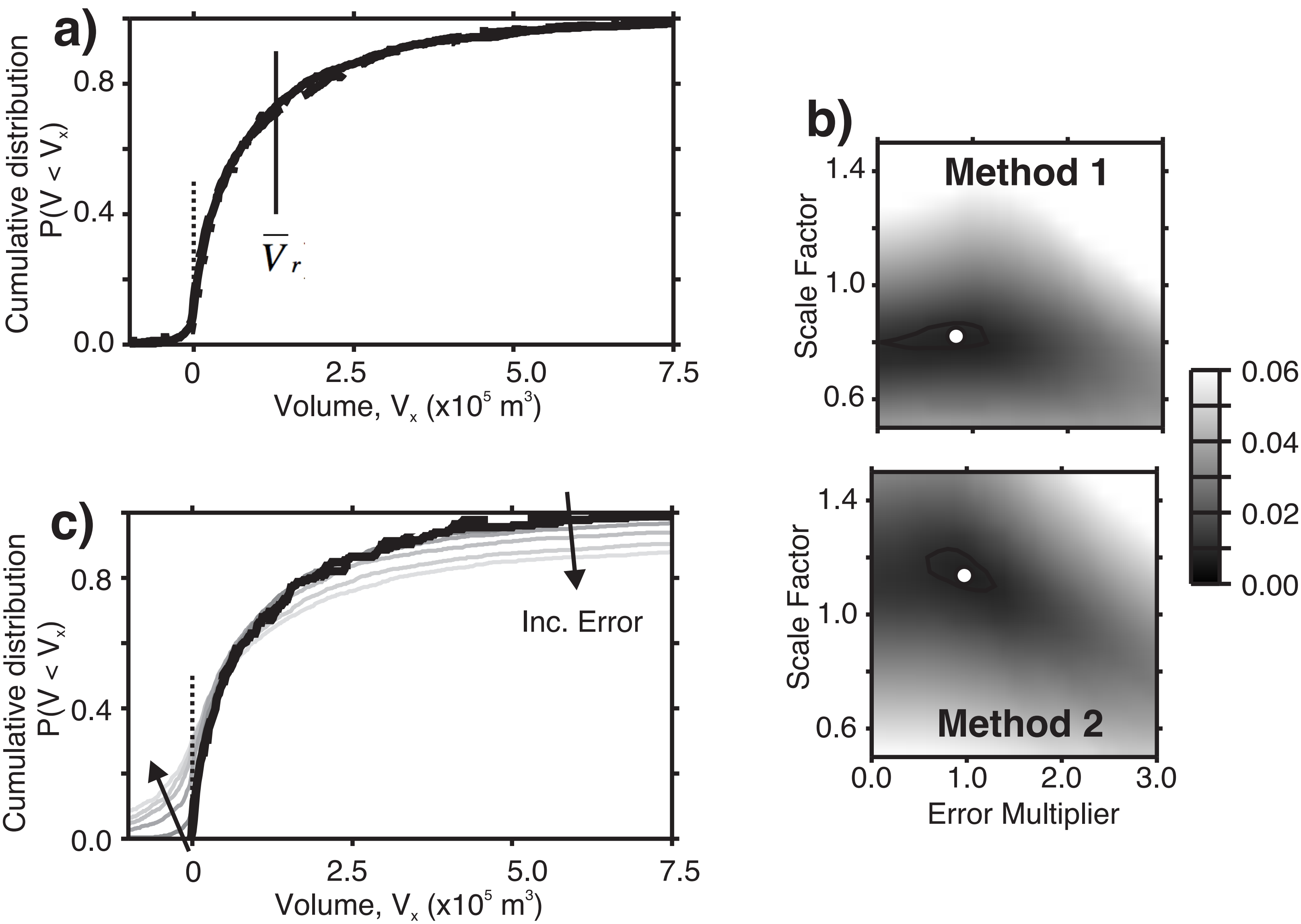

FIG 13

Figure 14

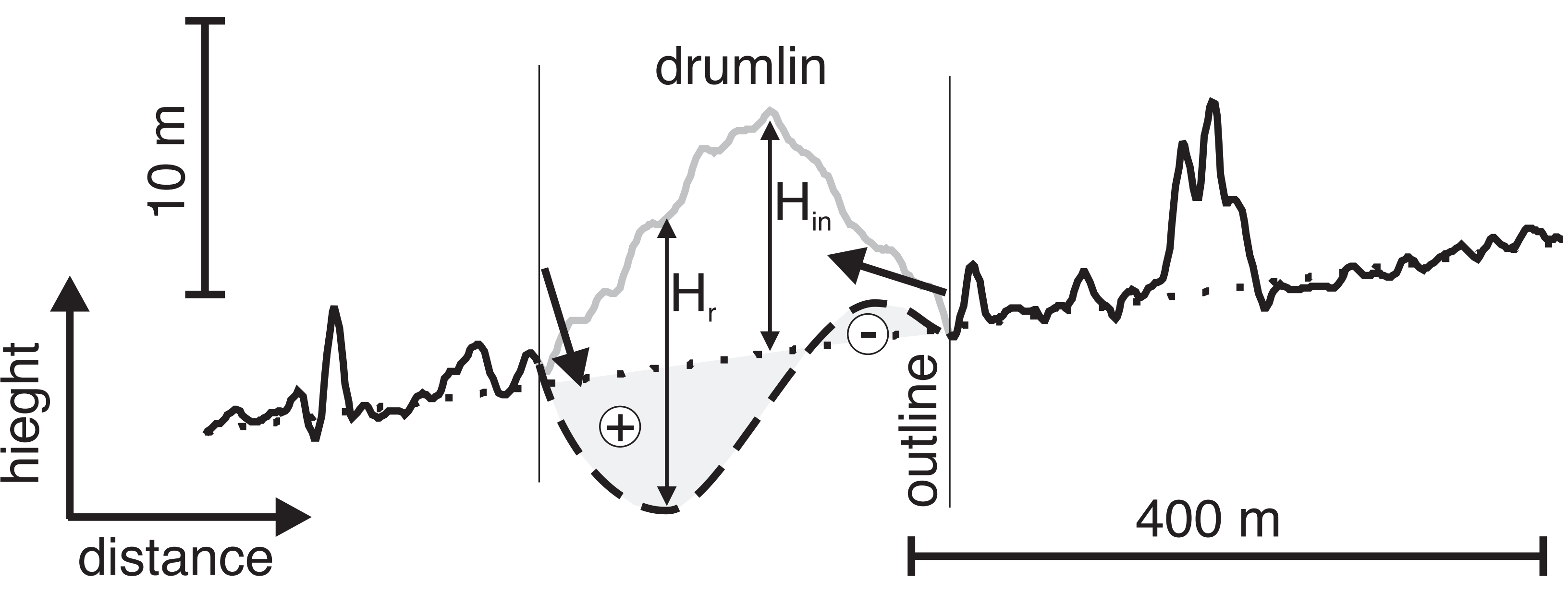

FIG 14